*Geological Magazine*

**www.cambridge.org/geo**

# Petrogenesis of a rare Ediacaran tonalite–trondhjemite–granodiorite suite, Egypt, and implications for Neoproterozoic Gondwana assembly

Abdel-Fattah M Abdel-Rahman

Department of Geology, American University of Beirut, PO Box 11-0236, Bliss Street, Beirut, Lebanon

**Original Article**

**Cite this article:** Abdel-Rahman A-FM (2021) Petrogenesis of a rare Ediacaran tonalite–trondhjemite–granodiorite suite, Egypt, and implications for Neoproterozoic Gondwana assembly. *Geological Magazine* **158**: 701–722. https://doi.org/10.1017/S0016756820000795

Received: 20 December 2019
Revised: 28 June 2020
Accepted: 5 July 2020
First published online: 13 August 2020

**Keywords:**
Ediacaran TTG from Egypt; Sr–Nd isotope geochemistry; U–Pb zircon TIMS age; petrogenesis; Gondwana assembly

**Author for correspondence:**
Abdel-Fattah M. Abdel-Rahman,
Email: arahman@aub.edu.lb

## Abstract

Most tonalite–trondhjemite–granodiorite (TTG) suites are Archean–Palaeoproterozoic in age, but those of Neoproterozoic–Phanerozoic age are scarce. A rare Ediacaran high-Al TTG suite has been identified at the Fannani Igneous Complex (FIC) in the northern Arabian–Nubian Shield, which is essentially composed of amalgamated Neoproterozoic island-arc Pan-African composite terranes that contain several ophiolitic sutures. The FIC exhibits a wide range of $SiO_2$, $Al_2O_3$, Sr and Zr, shows moderate rare earth element (REE) enrichment, and K, Ti, Nb, Y and heavy REE depletion. It is a subsolvus suite with clear orogenic affinities and strong arc-geochemical signatures. The precise U–Pb zircon thermal ionization mass spectrometry age obtained (607.4 ± 1.95 Ma) indicates oceanic subduction extended to late stages of the East African Orogeny. The FIC exhibits $^{87}Sr/^{86}Sr$ compositions of 0.70346–0.71091 ($Sr_{(i)}$ ratio, 0.70284), and $^{143}Nd/^{144}Nd$ of 0.51254–0.51270 ($\epsilon_{Nd}(t) = +5.12$ to $+7.16$), typical of modern oceanic-arc rocks (as Japan-arc basalts), and suggestive of mantle sources and island-arc settings. The FIC possesses low values of Yb (1.55 ppm), Nb (14 ppm) and Y (24 ppm), and high ratios of Sr/Y (27), Zr/Sm (46) and Nb/Ta (11.8), typical of magmas produced by anatexis of a basaltic slab. Partial melting models show that the FIC magma was generated by melting ($F = 0.25–0.50$) of a subducted oceanic crust transformed into eclogite, leaving 10–25% garnet in the residue. The FIC and similar complexes produced via slab melting during the closure of the Mozambique Ocean formed large juvenile belts along the East African Orogen that sutured East and West Gondwana together into a united supercontinent.

## 1. Introduction

Trondhjemite–tonalite–granodiorite (TTG) rocks are juvenile plutonic suites of intermediate to felsic compositions (essentially primitive granitoids) that have some geochemical similarities to adakites; TTGs have also been referred to as low-Mg adakites (Rapp *et al.* 1999; Condie, 2005). Adakites have been described as arc-volcanic and plutonic rocks characterized by relatively high Mg no., high Sr/Y, high La/Yb and low Zr/Sm ratios, relatively enriched in compatible transition elements (such as Mg, Ni, Cr and V), with their chemistry reflecting extensive interaction of the ascending melt (of a subducted oceanic slab) with mantle peridotite, unlike magmas that produce TTGs (Defant & Drummond, 1990; Martin, 1999; Rapp *et al.* 1999; Condie, 2005; Martin *et al.* 2005; Castillo, 2006, 2008, 2012; Moyen, 2009; Cox *et al.* 2019). As summarized by Condie (2005), although adakites have some similar geochemical characteristics to TTGs, adakites are more mafic and have Mg no. > 0.5, Sr > 500 ppm (often > 1000 ppm), Cr > 50 ppm and Ni > 20 ppm. Given the volume of TTG lithologies, forming about 50% of preserved Archean terrains, and their significance in understanding the origin and early evolution of continental masses, numerous studies of TTGs have been carried out (e.g. Barker, 1979; Martin, 1987; Condie, 1998; Smithies & Champion, 2000; Souza *et al.* 2001; Foley *et al.* 2002; Condie, 2005; Martin *et al.* 2005; Bédard, 2006; Moyen *et al.* 2007; Nair & Chacko, 2008; Senshu *et al.* 2009; Huang *et al.* 2010; Moyen, 2011; Nagel *et al.* 2012; Moyen & Martin, 2012; van Hunen & Moyen, 2012; Almeida *et al.* 2017).

A valuable body of experimental work on the generation of tonalitic–trondhjemitic melts has become available since the pioneering earlier studies of Green & Ringwood (1968), Green (1972) and Marsh & Carmichael (1974). Rapp *et al.* (1988) showed that 10–20% partial melting of low-K tholeiite via Hb-dehydration melting (at 16–22 kbar and 1100°C) produced high-Al TTG liquids. Wolf & Wyllie (1989) demonstrated that vapour-absent (dehydration) melting of low-K olivine tholeiitic composition (natural amphibolites) at 10 kbar and 750–975°C produced high-Al tonalities with a Hb–Gnt-rich residue. Drummond & Defant (1990) indicated that partial melting of a subducted basaltic slab under eclogitic to garnet–amphibolitic conditions ($P = 23–26$ kbar; $T = 700–775$°C) generates high-Al TTG suites. Several other



CAMBRIDGE UNIVERSITY PRESS

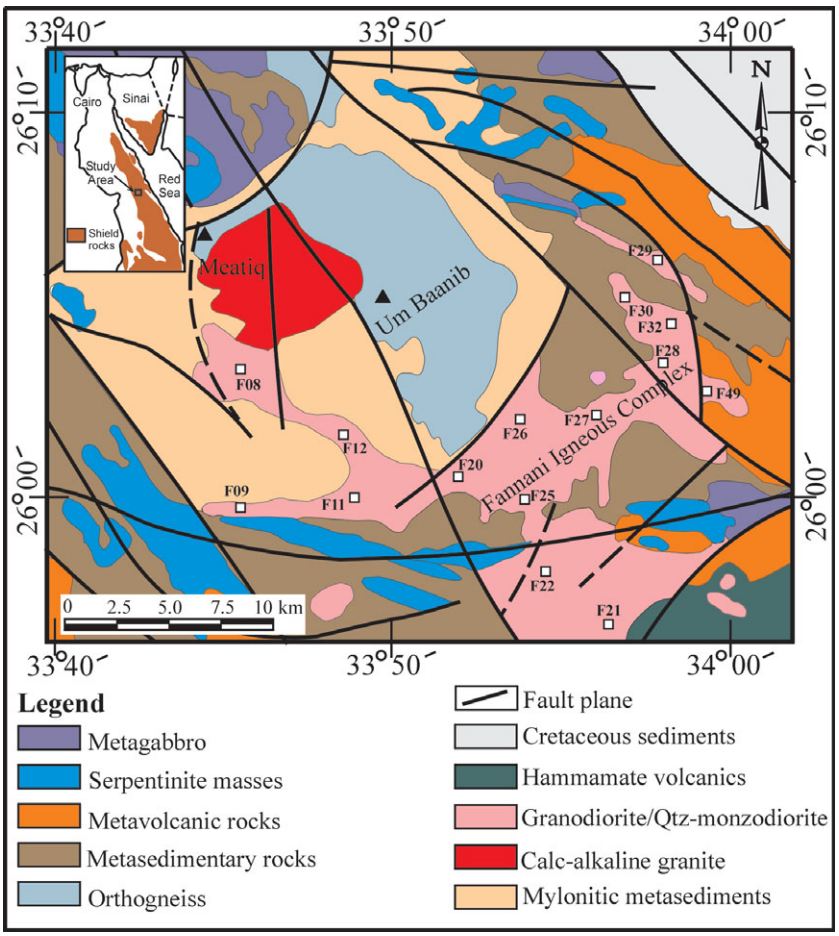


**Fig. 1.** (Colour online) Geological map of the region containing the Meatiq metamorphic core complex of eastern Egypt, showing the exposures of the investigated Fannani Igneous Complex that cross-cuts rock units of both the metasedimentary succession and the ophiolitic assemblage, as well as the Um Baanib orthogneiss dome. The map is modified from El-Ramly (1972), El-Gaby *et al.* (1984) and Neumayr *et al.* (1996). Sample locations are marked by squares. Inset is a location map.

experimental studies showed that melting of eclogites and amphibolites have produced melts of TTG compositions (e.g. Rapp *et al.* 1991; Winther, 1996; Wylie *et al.* 1997; Prouteau *et al.* 2001) and, as amphibole disappears relatively quickly during melting, the liquid produced would be in equilibrium with an amphibole-free assemblage (Gnt+Cpx), which is actually eclogitic (Moyen & Stevens, 2006; Laurie & Stevens, 2012). Since these and other experimental studies confirmed that melting of a subducted basaltic slab produces TTG suites, there is a strong link between TTGs and active subduction (e.g. Moyen & Martin, 2012). Accordingly, this study can be used to track subduction in the northernmost part of the Arabian–Nubian Shield (ANS) during the very late stages of the East African Orogen (EAO), for which the tectonic regime is still highly debatable.

Unaltered magmatic complexes exposed in NE Africa and Arabia form the best well-preserved Neoproterozoic terrains worldwide. These terrains encompass the vast ANS, which in itself is composed of amalgamated island-arc terranes and ophiolitic sutures, representing the northern segment of the EAO (Stern, 1994) that extends from Mozambique, Madagascar, Ethiopia, Somalia and Eritrea, N-wards into Sudan, western Arabia, eastern Egypt, Sinai, southern Israel and Jordan. East and west Gondwana were sutured along the EAO. The ANS forms the largest crustal segment of the Pan-African mobile belt that girdles Africa; some authors, including Hoffman (1999) and Meert & Lieberman (2008), considered these Pan-African terrains to represent valuable archives of what has been considered as one of the most remarkable orogenic episodes in all of Earth's history. It has been well-established that most TTG suites are of Archean–Palaeoproterozoic age, whereas Neoproterozoic TTGs are generally very scarce, with only a very few studies reported in the literature on TTG rocks occurring within the ANS. In this respect, a rare Neoproterozoic TTG suite has been identified at Mount Abu Fannani of eastern Egypt (Fig. 1), which is the subject of this contribution. Numerous investigations of other magmatic complexes within the northern part of the ANS have been carried out (e.g. Bentor, 1985; Abdel-Rahman & Doig, 1987; Abdel-Rahman & Martin, 1987; Abdel-Rahman, 1990, 1995, 1996, 2010, 2016, 2019; El-Shazly & El-Sayed, 2000; Loizenbauer *et al.* 2001; El-Sayed *et al.* 2004; Eliwa *et al.* 2006; Abdel-Rahman *et al.* 2009; Bea *et al.* 2009; Be'eri-Shlevin *et al.* 2009, 2011; Johnson *et al.* 2011; Maurice *et al.* 2012; Fritz *et al.* 2013; Jarrar *et al.* 2013; Eyal *et al.* 2014, 2019; Robinson *et al.* 2014; Elisha *et al.* 2017, 2019).

These, along with other investigations, have indicated that the nature of the tectonomagmatic environment in the northern segment of the EAO at *c.* 600 Ma is debatable. While some authors interpreted the Ediacaran magmatic activity in the ANS to have occurred in a post-collisional to extensional regime (e.g. Be'eri-Shlevin *et al.* 2011; Jarrar *et al.* 2013; Elisha *et al.*

https://doi.org/10.1017/S0016756820000795 Published online by Cambridge University Press

2017, 2019; Eyal *et al.* 2019), others suggested that such magmatism is subduction-related and developed during the very late orogenic stages of the EAO (e.g. Bentor, 1985; Doebrich *et al.* 2007; Johnson *et al.* 2011; Abu El-Enen & Whitehouse, 2013; Robinson *et al.* 2014). The occurrence of TTG suites is considered to be one of the best markers for active subduction, and the discovery of this rare Ediacaran TTG suite of the Fannani Igneous Complex (FIC) can be used to shed light on this debatable and controversial issue. In addition, this study will provide basic petrological, geochemical and isotopic data on the FIC, determine its age of emplacement, and assess the petrogenetic processes involved. The data will also be used to evaluate the role of Pan-African TTG magmatism in shield evolution and in Neoproterozoic Gondwana assembly in the context of the regional geodynamic framework. In brief, the investigated TTG suite may have significant tectonomagmatic implications, and can help to redraw the sequence of events during the very late stages of the EAO.

## 2. The geological context

### 2.a. Regional geology and nature of host rocks

Shield rocks that make up most of the ANS consist predominantly of Pan-African orogenic plutonic and coeval volcanic assemblages developed essentially during the Neoproterozoic Era (*c.* 870–520 Ma; Shackleton, 1996; Wilson *et al.* 1997). These assemblages occur within a mobile belt representing accreted island-arc terrains. As a result of the EAO, subduction and piling of thrust sheets were probably the principal processes of crustal accretion that was followed by some post-tectonic magmatism associated with mountain decay in east Africa and Arabia during the Neoproterozoic Era (e.g. Johnson *et al.* 2011). The occurrence of several older (*c.* 810–700 Ma) ophiolitic sutures (e.g. Berhe, 1990; Ali *et al.* 2010) across the ANS, including the Fawakhir ophiolite that hosts the FIC, is consistent with shield development on an oceanic crust by the juxtaposition of a series of island arcs (Abdel-Rahman, 1995, 1996; Blasband *et al.* 2000; Loizenbauer *et al.* 2001; Jarrar *et al.* 2003; Johnson & Woldehaimanot, 2003; El-Sayed *et al.* 2004; Abdel-Rahman *et al.* 2009; Johnson *et al.* 2011; El-Bialy, 2013; Robinson *et al.* 2014, 2015; Elisha *et al.* 2017, 2019; Cox *et al.* 2019; Eyal *et al.* 2019).

The region encompassing the FIC hosts one of the few metamorphic domes exposed in eastern Egypt, known as the 'Meatiq' core complex. Several studies focusing on the structural, tectonic and metamorphic evolution of this Meatiq core complex have been carried out by a large number of authors (Hume, 1934; Neubauer, 1962; Schurmann, 1966; Akaad & Noweir, 1969; Akaad & Shazly, 1972, 1975; El-Gaby, 1976; El-Shazly & Essawy, 1978; Habib *et al.* 1985; Greiling *et al.* 1994; Neumayr *et al.* 1996, 1998; El-Sayed *et al.* 1999; Loizenbauer *et al.* 2001; Andresen *et al.* 2009, 2010; Fritz *et al.* 2014). The Meatiq dome is made up of granitic orthogneiss occurring at the structurally lowest part, overlain by a dominant metasedimentary succession consisting of quartz-rich schists intercalated with metapelitic schists. The metasedimentary succession is tectonically overlain by Fawakhir ophiolitic nappes and island-arc volcanic rocks (e.g. El-Sayed *et al.* 1999) that were obducted along low-angle thrust planes (El-Gaby *et al.* 1990; Neumayr *et al.* 1996; Loizenbauer *et al.* 2001).

The Meatiq rocks were described as variably cataclastic orthogneiss (granite gneisses) locally hosting amphibolite lenses, mylonites, phyllonites, augen schists and mylonitic amphibolites (Habib *et al.* 1985). Andresen *et al.* (2010) indicated that the core of the dome consists of coarse-grained, foliated orthogneisses (the Um Baanib orthogneiss), which structurally upwards become gradually more mylonitized and fine-grained, forming a garnet-bearing mylonitic carapace. The orthogneiss was considered by El-Ramly *et al.* (1984) and Greiling *et al.* (1984) to represent variably deformed calc-alkaline juvenile igneous rocks associated with the EAO. Sturchio *et al.* (1983) proposed a protolith age of *c.* 626 Ma for the orthogneiss, whereas Loizenbauer *et al.* (2001) interpreted it to be as old as 780–800 Ma, possibly involving even older material, and suggested that the gneiss-forming event occurred at *c.* 660–640 Ma. According to Fritz *et al.* (1996), the updoming of the Meatiq basement is constrained by $^{40}Ar/^{39}Ar$ dating of micas at 595.9 ± 0.5 Ma. Andresen *et al.* (2009) carried out a comprehensive geochronological study on the Meatiq metamorphic dome and surrounding metasedimentary and ophiolitic rock units; they considered the formation of this gneiss dome to be a young (631 Ma) structural feature formed as a result of NE–SW shortening contemporaneous with folding of the nearby Hammamat sediments at *c.* 605–600 Ma during oblique collision of East and West Gondwana. Andresen *et al.* (2009) also included a sample from the FIC, which they referred to as "Abu Ziran syn-tectonic diorite", considering it to have an age of 609.0 ± 1.0 Ma to 605.8 ± 0.9 Ma. A study on magmatic and solid state structures of these Abu Ziran rocks was carried out by Fritz *et al.* (2014); they indicated that extensional shear was developed at *c.* 585 Ma, and that extension was accompanied by exhumation of the Meatiq dome, which took place soon after the solidification of the so-called 'Abu Ziran' granitic rocks. The Meatiq gneiss dome was intruded by a younger calc-alkaline granitic phase (the 'Arieki' granite) dated by Andresen *et al.* (2009) at 590.5 ± 3 Ma.

Several investigations were carried out on the Fawakhir ophiolitic assemblage; it is considered to occur as tectonically dismembered sheets, blocks and fragments, and is represented by ultramafic serpentinites variably altered into talc-carbonates, metagabbros, massive but locally sheeted mafic dykes, and locally pillowed metabasalts (Akaad & Noweir, 1969; Nasseef *et al.* 1980; Church, 1988; Abdel-Rahman *et al.* 2009). These rock units were described as ophiolitic melange (e.g. Shackleton *et al.* 1980; Ries *et al.* 1983) embedded in the metasedimentary succession, were first dated at 813–777 Ma (Pb–Pb, zircon) by Loizenbauer *et al.* (2001), and were interpreted to represent a segment of oceanic crust formed in a marginal (back-arc) basin, similar to the Wadi Ghadir ophiolite occurring further south (El-Gaby *et al.* 1988; El-Sayed *et al.* 1999). In contrast, Andresen *et al.* (2009) implied that the Fawakhir ophiolite possibly formed in a fore-arc setting, and reported a (more realistic) U–Pb zircon thermal ionization mass spectrometry (TIMS) age of 736.5 ± 1.2 Ma. Abdel-Rahman *et al.* (2009) considered it to be a Penrose-type ophiolite sequence, indicating that its magmas appear to have been derived from a depleted (normal mid-ocean ridge basalt, or N-MORB, -like) mantle source. Despite the abovementioned in-depth structural, tectonic and metamorphic studies that were carried out on the various rock formations of the region encompassing the FIC, no detailed petrological-geochemical studies on the FIC are available in the literature.

### 2.b. Field relationships and megascopic appearance

The FIC occurs along the Qusair–Qena road, and is located some 70 km to the west of the Red Sea coastal city of Qusair at latitude 26° 00′ N, longitude 33° 50′ E. It forms low-lying, deeply eroded

https://doi.org/10.1017/S0016756820000795 Published online by Cambridge University Press

terrains, with its outcrops displaying highly irregular and relatively complex margins, and with tongues extending into the enclosing metasedimentary and metavolcanic units (Fig. 1). The exposures of this magmatic body extend to an overall length of about 30 km but with a highly variable width, estimated to be about 12 km on average. Due to the lack of vegetation and overburden, the FIC is well-exposed. Overall, it is made up essentially of monotonous greyish-white, medium- to coarse-grained, predominantly granodioritic rocks, showing non-porphyritic as well as porphyritic textures, but with a minor quartz-monzodioritic variety occurring further east within this intrusion. Mineralogical and textural variations between granodiorites and the much less abundant quartz-monzodioritic variety are gradational, and essentially related to differences in the proportion of mafic minerals. Parts of the FIC exhibit weak magmatic-flow textures represented by the alignment of some hornblende, biotite and/or idiomorphic plagioclase crystals. Late aplitic dykes derived from the FIC magma, as well as some rare quartz veins, are occasionally present in this complex. In general, the overall textural and mineralogical primary magmatic features of the FIC are well-preserved.

The FIC was essentially intruded between ophiolitic melange embedded in a metasedimentary succession consisting of low (greenschist) grade metamorphosed volcano-sedimentary sequences and Fawakhir ophiolitic lithologies (736 Ma; Andresen *et al.* 2009) to the south, and high-grade orthogneiss (631 Ma; Andresen *et al.* 2009) mantled by dominantly mylonitic metasediments, consisting of quartz-rich schists intercalated with metapelitic schists, forming the Meatiq gneiss dome to the north (Fig. 1). Thus, the FIC was emplaced at the southern periphery of this Meatiq dome and cross-cuts right into its centre, but at its southern margin it intruded the serpentinite and/or metagabbro ophiolitic assemblage, as well as the metasedimentary succession.

Field relationships reflect that the FIC exhibits both faulted contacts, as well as discordant irregular contacts with its host rocks, with some mafic xenoliths (from host rocks) occurring within this intrusion near its northern margin. Furthermore, the emplacement of the FIC caused contact metamorphism along its southern as well as northern margins, with a very narrow thermal aureole developed at its northern contact with the relatively high-grade host rocks of the Meatiq dome, and a relatively wider thermal aureole developed within the lower-grade metasedimentary succession in the south. The FIC and its host rocks are dissected by several NW-trending and ENE-trending faults. A total of 14 rock samples were collected across this magmatic complex, covering its entire length of about 30 km from west to east with its variable width and irregularly shaped boundaries.

## 3. Petrography

The FIC contains medium- to coarse-grained, equigranular to inequigranular rocks (Fig. 2), having both a non-porphyritic as well as a porphyritic variety. In the latter variety, plagioclase is the main phenocryst phase. As shown in Figure 2, the rocks consist of variable contents of plagioclase (37–52 vol%), quartz (18–29 vol%), K-feldspar (8–21 vol%), amphibole (2–25 vol%), biotite (2–16 vol%), epidote (1–4 vol%), muscovite (0–4 vol%) and opaque Fe–Ti oxides (2 vol%), and traces of accessory titanite, apatite, zircon and rare allanite. Plagioclase forms predominantly large idiomorphic grains (Fig. 2a–c), occasionally showing hypidiomorphic overgrowth features; it is rarely zoned, and exhibits Albite-, Carlsbad- and complex twinning. The K-feldspar is a relatively less abundant phase forming allotriomorphic perthitic grains. Amphibole is commonly pleochroic (yellowish beige to bluish green; Fig. 2a, b), forming idiomorphic to hypidiomorphic large grains, occasionally showing simple twinning and containing inclusions of quartz, titanite, magnetite and apatite. Biotite forms idiomorphic to hypidiomorphic grains (Fig. 2c–f) and exhibits greenish, beige and reddish-brown colours. Muscovite occurs in some of the more felsic lithologies and represents a minor constituent of these rocks. Epidote is present in most of the FIC samples (Fig. 2c–f), occurring predominantly as idiomorphic crystals, and also in the form of allotriomorphic rounded grains. Titanite is an abundant accessory phase that forms wedge-shaped to rectangular as well as allotriomorphic grains (Fig. 2c, e). Zircon and apatite are somewhat less common, and occur as tiny crystals. Allanite is rarely present within some epidote grains. Opaque phases are represented by magnetite and ilmenite. Most samples are generally fresh, with only a few samples showing minor alteration of some plagioclase grains to kaolinite or sericite and some amphibole and/or biotite to secondary chlorite. Signs of rock–fluid interaction at the post-magmatic or subsolidus stage are therefore rare.

Magmatic epidote has been reported in a number of igneous complexes (e.g. Evans & Vance, 1987; Farrow & Barr, 1992; Franz & Smelik, 1995; Barr *et al.* 2001; Dahlquist, 2001; Popov *et al.* 2001; Bédard, 2003; Bea *et al.* 2009; Abdel-Rahman, 2016; Cox *et al.* 2019). As indicated above, most samples of the FIC contain epidote, occurring as high-relief, weakly pleochroic, greenish-yellow, idiomorphic grains, commonly having patchy colour distribution (Fig. 2c–f). Epidote varies from 1 to 4 vol% of the rock. Many idiomorphic epidote grains exhibit well-developed crystals showing typical monoclinic crystal forms (Fig. 2d). It predominantly shows sharp euhedral contacts against biotite (Fig. 2c–f), but exhibits embayed to myrmekitic grain boundaries when in contact with feldspars and quartz (Fig. 2e, f). Epidote intergrown with quartz within resorption textures growing into the amphibole is also present. Textural features of the FIC epidote reported here (Fig. 2) are similar to those interpreted by Zen & Hammarstorm (1984) and Schmidt & Poli (2004) to represent features typical of magmatic epidote. Thus, epidote present in the FIC is inferred to be of igneous origin. The fresh appearance of plagioclase and the lack of biotite or amphibole alternation in rocks of the FIC further support this inference. Magmatic epidote reported in this study represents a somewhat rare occurrence within the vast ANS. In fact, only a few occurrences of magmatic epidote within this shield have previously been reported. In their study on Mount Moneiga quartz-dioritic pluton (844 Ma) in southern Sinai, Bea *et al.* (2009) reported the presence of some magnetite-plagioclase aggregates having a core of epidote that "seems to be of magmatic origin". Abdel-Rahman (2016) documented the presence of magmatic epidote in the TTG suite of the Mons Claudianus batholith (664 Ma) of eastern Egypt. Cox *et al.* (2019) reported magmatic epidote in adakites from the eastern part of the ANS. It should be noted that only a few studies have been carried out on adakites occurring within the ANS (e.g. Eliwa *et al.* 2006; Cox *et al.* 2019). Using the proportions of their mineralogical constituents (quartz, alkali-feldspar, plagioclase) on the IUGS classification diagram of Le Bas & Streckeisen (1991), 11 rock samples of the FIC plot in the field of granodiorite and only 3 (F-25, F-26 and F-32) plot in the quartz-monzodiorite field (Fig. 3).

https://doi.org/10.1017/S0016756820000795 Published online by Cambridge University Press

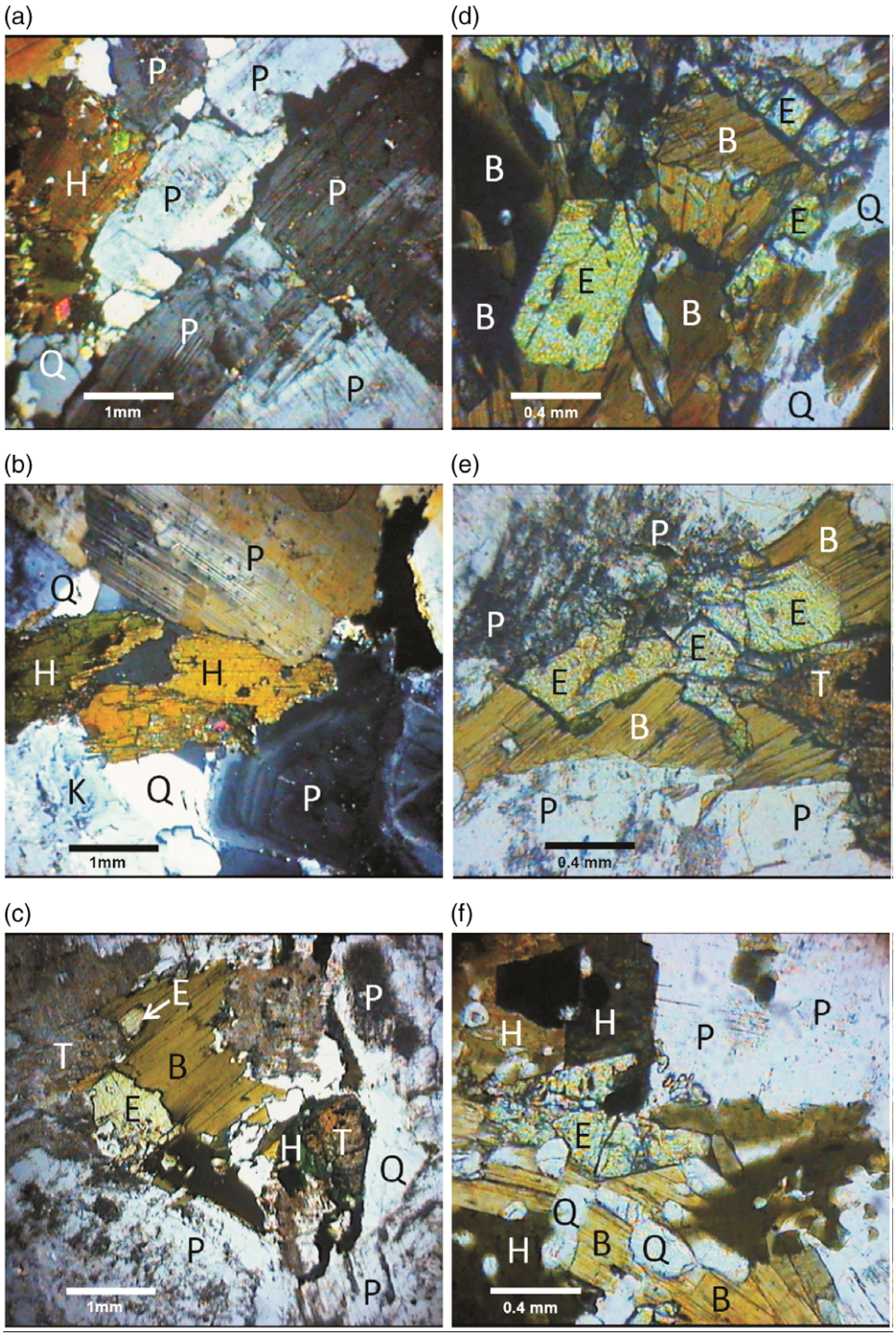


**Fig. 2.** (Colour online) Photomicrographs showing textures and mineralogical constituents of rocks of the FIC, as well as various features of magmatic epidote occurring in association with various mineral phases. (a–c) Abundant idiomorphic prismatic plagioclase crystals with allotriomorphic to hypidiomorphic quartz, K-feldspar, hornblende and biotite occupying the interstitial space, thus forming equigranular to inequigranular mosaic in various samples (F-26 (a) and F-25 (b) under cross-polarized light, with F-27 (c) under plane-polarized light). Photomicrograph (c), in particular, shows an abundance of the accessory phase titanite, and some idiomorphic epidote grains armouring around pristine biotite and displaying predominantly sharp euhedral contacts against it. (d) Well-developed monoclinic epidote crystals, showing sharp idiomorphic contacts with biotite (sample F-26; plane-polarized light). (e) Several blocky idiomorphic epidote grains showing sharp euhedral contacts with biotite, but embayed against plagioclase; accessory titanite is also present (sample F-27; plane-polarized light). (f) Cross-section of idiomorphic epidote crystal intergrown with quartz and in sharp contact with biotite, but embayed against both hornblende and plagioclase (sample F-26; plane-polarized light). Note the predominantly fresh appearance and unaltered nature of the various mineral phases present in all photomicrographs. P – plagioclase; Q – quartz; K – K-feldspar; B – biotite; H – hornblende; E – epidote; T – titanite.

https://doi.org/10.1017/S0016756820000795 Published online by Cambridge University Press

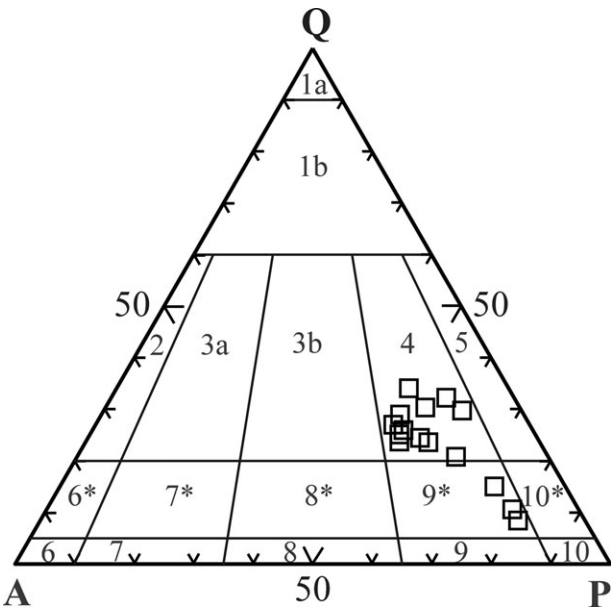


**Fig. 3.** The IUGS classification diagram (after Le Bas & Streckeisen 1991) for rocks of the Fannani Igneous Complex (FIC); all data points plot in the fields of granodiorite and quartz-monzodiorite.

## 4. Analytical methods

### 4.a. Geochemistry: major elements

Chemical data have been obtained on 14 representative samples from the FIC. Concentrations of the major elements were determined on whole-rock powders fused with lithium-metaborate in discs by X-ray fluorescence spectrometry (Phillips PW1400 Spectrometer model 691, at McGill University) using a Rh tube operated at 40 kV and 70 mA. Loss on ignition (LOI) was determined by heating powdered samples for 50 minutes at 1000°C.

### 4.b. Trace elements

Concentrations of trace elements including V, Ni, Rb, Sr, Ba, Zr, Nb, Y, Ga, Th and U for the same 14 whole-rock samples were determined on pressed pellets by X-ray fluorescence (operating conditions: Rh radiation, 70 kV, 40 mA). The analytical precision, as calculated from 20 replicate analyses of one sample, is better than 1% for most major elements and better than 5% for most trace elements. The detection limit for the trace elements analysed is 1 ppm.

### 4.c. Rare earth elements, hafnium and tantalum

Hafnium, tantalum and 14 rare earth elements (REEs) were analysed for five representative samples from the FIC. The concentrations of these elements were determined by inductively coupled plasma mass spectrometry (ICP-MS) at the Activation Laboratories (Ontario, Canada). Solutions of fused samples are spiked with three internal standards to cover the entire mass range. These are further diluted and are introduced into a Perkin Elmer-SCIEX Elan 6000 ICP-MS using a proprietary sample introduction methodology. The primitive mantle values used for normalization are those of Sun & McDonough (1989).

### 4.d. Radiogenic isotope ratios

#### 4.d.1. U–Pb zircon (TIMS) analysis

An absolute age for the FIC was determined on a pristine rock sample (F-27) using the U–Pb zircon TIMS method. Zircon grains were separated from the sample, and the grains were treated before the analysis. In order to overcome the effects of radioactive-decay-induced crystal defects and associated lead loss resulting in discordant analyses, zircon grains are pre-treated by the method of thermal annealing and chemical leaching (Mattinson, 2005). This method involves heating of the zircon inside a furnace at 900°C for 60 hours. The annealed grains selected for analysis were subsequently loaded into fluorinated ethylene propylene (FEP) Teflon microcapsules and leached in concentrated hydrofluoric acid (HF) at 180°C within high-pressure vessels for 12 hours. The partially dissolved sample is then transferred into Savillex FEP breakers for rinsing. The leached material is decanted with several millilitres of ultra-pure water and by fluxing successively with 4 N $HNO_3$ and 6 N HCl on a hot plate and/or in an ultrasonic bath. After final rinsing with ultra-pure water, zircon grains are loaded back into microcapsules, spiked with mixed $^{205}Pb$–$^{233}U$–$^{235}U$ tracer solution and dissolved completely in concentrated HF at 220°C for 48–60 hours. Essentially, the high-U parts of the zircon crystals that are associated with Pb loss are preferentially removed, leaving a residue of relatively low-U content. Isotope compositions were measured on the VG Sector 54 multi-collector TIMS at the Activation Laboratories (Ontario, Canada). The measured isotopic ratios were corrected for mass-dependent isotope fractionation in the mass spectrometer, as well as for U and Pb contributions from the spike, laboratory blanks and initial Pb in the sample. Common-Pb corrections were calculated by using the model of Stacey & Kramers (1975) and the interpreted age of the sample. All common Pb in the analyses was assigned to procedural blank with a measured composition of $^{206}Pb/^{204}Pb = 18.31 \pm 0.53$, $^{207}Pb/^{204}Pb = 15.38 \pm 0.35$, $^{208}Pb/^{204}Pb = 37.45 \pm 1.1$ ($2\sigma$); total procedural blanks were $< 0.5$ pg for Pb and $< 0.1$ pg for U. It should be noted that the ID TIMS method was used for analysis and isotopic measurements were made against a calibrated isotopic tracer, with precisely determined concentrations and isotopic compositions as given in Condon *et al.* (2015) and McLean *et al.* (2015). Age calculations are based on the decay constants of Steiger & Jäger (1977).

#### 4.d.2. Sm–Nd isotope analysis

Five representative whole-rock samples from the FIC have been used for the Sm–Nd isotopic analysis carried out at the Activation Laboratories (Ontario, Canada). Rock powders of these samples were dissolved in a mixture of HF, $HNO_3$ and $HClO_4$. Before the decomposition, the samples were totally spiked with $^{149}Sm$–$^{146}Nd$ mixed solution. The REEs were separated using conventional cation-exchange techniques. Both Sm and Nd were separated by extraction chromatography on HDEHP-covered Teflon powder. The various Sm–Nd isotopic ratios were measured using a Triton-MC mass spectrometer. Accuracy of the measurements of Sm and Nd contents were ±0.5%, and for $^{147}Sm/^{144}Nd$ ±0.5% ($2\sigma$). The various $^{143}Nd/^{144}Nd$ ratios measured for rocks of the FIC are relative to the value of 0.511860 of the La Jolla Nd standard.

https://doi.org/10.1017/S0016756820000795 Published online by Cambridge University Press

#### 4.d.3. Rb–Sr isotope analysis

For the Rb–Sr isotopic analysis, five whole-rock samples were dissolved in a mixture of HF, $HNO_3$ and $HClO_4$. Before the decomposition, the samples were totally spiked with $^{85}Rb$–$^{84}Sr$ mixed solution. Rb and Sr were separated using conventional cation-exchange techniques. Total blank are 0.01–0.05 ng for Rb and 0.3–0.7 ng for Sr. The various Rb–Sr isotopic ratios were measured using a Triton-MC mass spectrometer. The accuracy of the measurements of Rb and Sr contents were ±0.5% and for $^{87}Rb/^{86}Sr$ ±1.0% ($2\sigma$). The Sr isotopic ratios were normalized to the $^{88}Sr/^{86}Sr$ ratio of 8.37521.

## 5. Analytical results

### 5.a. Major- and trace-element geochemistry

Chemical data for 14 representative whole-rock samples from the FIC, expressed as major-element oxides (in wt%) and trace elements (in ppm) are given in Table 1. The concentrations of the rare earth elements (REEs) as well as Hf and Ta (in ppm) are listed in Table 2. Also given in Tables 1 and 2 are averages of Proterozoic TTG compositions from various regions worldwide, as compiled by Condie (2005). The chemical data show that rocks of the FIC span a wide range of compositions including $SiO_2$ (58.3–73.8 wt%), $Al_2O_3$ (13.5–18.6 wt%), CaO (0.92–5.2 wt%), Sr (88–1239 ppm), Rb (36–109 ppm) and Ba (251–929 ppm) (Tables 1, 2; Fig. 4). The rocks contain relatively low concentrations of MgO (average, 1.2 wt%) and $TiO_2$ (0.6 wt%), and low concentrations of high-field-strength elements (HFSEs) such as Nb (average, 14 ppm), Hf (6.1 ppm) and Ta (1.1 ppm), but are moderately enriched in Zr (250 ppm). Overall, depletion in Mg, Ti, Nb, Ta, Hf and the HREEs is a noticeable feature in the FIC rocks (Tables 1, 2).

On Harker-type diagrams, variations of silica versus some major- and trace-elements produce linear trends showing gradual decrease in $Al_2O_3$, CaO, $Fe_2O_3$ (as total iron), $TiO_2$, Sr and Ga with increasing silica contents, but with the alkalis and Y showing a slight positive correlation (Fig. 4). This is consistent with a sequence of crystallization (as deduced from textural observations) characterized by early formation of plagioclase (Fig. 2a, b), which also dominated the phenocryst phases in porphyritic varieties, followed by hornblende. The generally well-defined trends, with only limited scatter of data points, suggest a continuous process of evolution via internal differentiation. As indicated in the petrography section (Section 3), using the mineralogical constituents (quartz, albite, K-feldspar) in the IUGS classification diagram of Le Bas & Streckeisen (1991), rocks of the FIC plot largely in the fields of granodiorite (11 samples), with only three samples classified as quartz-monzodiorite (Fig. 3). Data points of the FIC occupy the fields of tonalite, trondhjemite granodiorite and granite (TTG; Fig. 5a) of O'Connor (1965) and Barker (1979). The rocks also plot within or around the field of quartz-diorite and continental trondhjemite (Fig. 5b), that is, distinct from the ophiolite-related oceanic plagiogranite field delineated by Coleman & Peterman (1975). In addition, most elemental averages of the investigated rocks (Tables 1, 2) compare rather well with averages of Proterozoic TTGs from various regions (reported in Condie, 2005). Elemental ratios of the FIC rocks are also somewhat similar to those of Proterozoic TTGs, which exhibit averages of $K_2O/Na_2O = 0.56$ (it is 0.61 in the FIC), $Sr/Y = 37$ (27 in the FIC) and $Nb/Ta = 9.9$ (11.8 in the FIC).

Many authors, including Barker *et al.* (1976), Barker & Arth (1976), Barker (1979) and Defant & Drummond (1990), have distinguished between a low-Al TTG-type (having < 15 wt% $Al_2O_3$ at 70 wt% $SiO_2$, < 200 ppm Sr, slightly enriched LREE, flat HREE with a negative Eu-anomaly) and a high-Al type (having $Al_2O_3$ contents > 15 wt% at 70 wt% $SiO_2$, high Sr > 300 ppm, low Yb < 1.8 ppm, low Nb < 11 ppm, low to moderate K/Rb ratios < 750, enriched LREEs, depleted HREEs, and have no, or only a slight, Eu anomaly). Rocks of the FIC do exhibit these chemical signatures, including high $Al_2O_3$ contents of 16.6 wt% at 70 wt% silica, thus representing a high-alumina TTG suite.

As shown in Figure 6a, all rock samples of the FIC are peraluminous in nature, with the exception of only one metaluminous sample. Overall, the FIC rocks are subsolvus (as revealed by their two feldspar mineralogy), having typical calc-alkaline affinities (Fig. 6b), and exhibit characteristic features of 'I-type' suites. Furthermore, the K/Rb versus Rb/Sr diagram (Fig. 7a) shows that the FIC rocks occupy the field of 'orogenic' complexes of Abdel-Rahman & El-Kibbi (2001), and the (Y + Nb) versus Rb diagram (Fig. 7b) indicates that these rocks are typical of 'volcanic-arc granites' of Pearce *et al.* (1984). On various inter-element variation diagrams, such as Rb/Sr versus both Rb/Zr and Sr (Fig. 8a, b), and Rb/Y versus Nb/Y (Fig. 8c), data points of the FIC show, despite some scatter, generally smooth covariations with linear trends, suggesting that internal differentiation produced the more-evolved lithologies of the investigated TTG suite.

### 5.b. Rare earth elements, hafnium and tantalum

Concentrations of the REEs as well as Ta and Hf in the FIC rocks are given in Table 2; these rocks exhibit moderate REE values (∑REE = 123 ppm, on average). The rocks are LREE enriched over HREE, as the latter show marked depletion (e.g. Yb = 1.55 ppm, on average), and this seems to be a characteristic feature for most TTG rocks in general (having Yb < 1.8 ppm). The primitive-mantle normalized REE patterns (Fig. 9a) are parallel to sub-parallel, moderately fractionated (mean $(La/Yb)_N = 12.8$)), and exhibit notable non-fractionated or flat HREEs. The REE profiles show no, or insignificant, Eu anomalies (Fig. 9a). Lack of Eu anomaly is consistent with the early crystallization of Na-rich plagioclase and its relative abundance in the FIC rocks (Fig. 2a, b). As noted by Drummond & Defant (1990), the lack of Eu anomaly appears to be a universal feature for high-Al TTGs. Rocks of the FIC exhibit low contents of Ta and Hf, with values ranging from 0.28 to 2.1 ppm and from 3.0 to 9.2 ppm, respectively. These values, along with the concentrations of the REEs, are comparable to those of Neoproterozoic TTG averages (Table 2). Overall features of some trace elements and REEs are summarized in a primitive-mantle-normalized spidergram for the FIC (Fig. 9b). The normalized multi-element profiles show moderate enrichment in some incompatible elements, and some depletion in HREEs and Nb; the profiles exhibit pronounced negative Nb anomaly, which is a typical feature of high-alumina TTG rocks.

Halla *et al.* (2009) subdivided TTG rocks into two groups (low-HREE and high-HREE), with the former characterized by low Mg, high Al, high Sr, high Nb/Ta ratio, low Yb and low HREE. The chemical composition of the FIC (with its marked HREE depletion and averages of MgO = 1.23 wt%, $Al_2O_3$ = 15.6 wt%, Sr = 479 ppm, Yb = 1.55 ppm, Nb/Ta = 11.8) indicate that it belongs to the low-HREE TTG group of Halla *et al.* (2009). The later authors

https://doi.org/10.1017/S0016756820000795 Published online by Cambridge University Press

**Table 1.** Major- and trace-element composition (in wt% and ppm, respectively) of representative TTG samples from the Fannani Igneous Complex (Egypt). $Fe_2O_3$* is total iron expressed as $Fe_2O_3$. Rock types based on the IUGS classification are granodiorite (GRD) and quartz monzodiorite (QMD)

| Rock sample no. | GRD F-08 | GRD F-09 | GRD F-11 | GRD F-12 | GRD F-20 | GRD F-21 | GRD F-22 | QMD F-25 | QMD F-26 | GRD F-27 | GRD F-28 | GRD F-30 | QMD F-32 | GRD F-49 | FIC average | TTG average |
|---|---|---|---|---|---|---|---|---|---|---|---|---|---|---|---|---|
| $SiO_2$ | 67.34 | 66.99 | 68.34 | 67.40 | 67.41 | 67.80 | 72.27 | 60.55 | 58.26 | 62.30 | 73.84 | 66.94 | 60.78 | 72.12 | 66.60 | 67.3 |
| $TiO_2$ | 0.619 | 0.62 | 0.512 | 0.645 | 0.599 | 0.526 | 0.207 | 0.784 | 0.937 | 0.718 | 0.155 | 0.681 | 1.13 | 0.27 | 0.60 | 0.47 |
| $Al_2O_3$ | 15.20 | 15.28 | 14.86 | 15.26 | 15.59 | 15.36 | 14.92 | 18.57 | 18.58 | 17.66 | 14.12 | 15.76 | 16.10 | 13.49 | 15.77 | 15.80 |
| $Fe_2O_3$* | 4.16 | 4.20 | 3.57 | 4.30 | 3.82 | 3.51 | 1.73 | 5.11 | 5.76 | 4.70 | 2.17 | 0.83 | 6.67 | 2.85 | 3.81 | 4.04 |
| MgO | 0.98 | 1.00 | 0.88 | 1.03 | 1.20 | 1.08 | 0.48 | 2.06 | 2.24 | 1.86 | 0.29 | 1.04 | 2.53 | 0.58 | 1.23 | 1.48 |
| MnO | 0.07 | 0.07 | 0.06 | 0.07 | 0.07 | 0.07 | 0.03 | 0.07 | 0.08 | 0.07 | 0.03 | 0.06 | 0.11 | 0.04 | 0.06 | 0.08 |
| CaO | 2.29 | 2.38 | 1.97 | 2.27 | 2.43 | 2.7 | 1.42 | 4.4 | 5.23 | 3.82 | 1.34 | 1.94 | 4.5 | 0.92 | 2.69 | 3.42 |
| $Na_2O$ | 4.39 | 4.4 | 4.34 | 4.38 | 4.87 | 4.72 | 4.88 | 5.84 | 5.58 | 5.58 | 4.79 | 5.18 | 4.14 | 5.43 | 4.89 | 4.33 |
| $K_2O$ | 3.76 | 3.95 | 3.93 | 3.98 | 3.39 | 3.28 | 3.58 | 2.08 | 1.73 | 2.31 | 2.81 | 1.95 | 2.59 | 2.74 | 3.01 | 2.3 |
| $P_2O_5$ | 0.205 | 0.21 | 0.164 | 0.216 | 0.22 | 0.203 | 0.078 | 0.274 | 0.359 | 0.25 | 0.023 | 0.182 | 0.294 | 0.06 | 0.20 | 0.14 |
| LOI | 1.25 | 0.67 | 0.98 | 0.6 | 0.41 | 0.86 | 0.45 | 0.62 | 1.28 | 0.83 | 0.6 | 1.13 | 1.28 | 1.34 | 0.88 | – |
| Total | 100.4 | 99.94 | 99.76 | 100.3 | 100.2 | 100.2 | 100.2 | 100.5 | 100.2 | 100.2 | 100.3 | 99.81 | 100.2 | 99.97 | 100.2 | 99.36 |
| V | 40 | 39 | 28 | 42 | 42 | 31 | 10 | 65 | 80 | 51 | 6 | 35 | 93 | 7 | 41 | – |
| Ni | 13 | 15 | 15 | 14 | 17 | 17 | 11 | 23 | 23 | 23 | 11 | 17 | 28 | 14 | 17 | 23 |
| Rb | 108 | 108 | 107 | 109 | 71.8 | 72.3 | 55.3 | 38.2 | 35.6 | 46.1 | 53.6 | 49.3 | 45.7 | 39.9 | 67 | 63 |
| Sr | 295 | 324 | 275 | 313 | 517 | 487 | 392 | 1081 | 1239 | 940 | 139 | 247 | 367 | 88 | 479 | 473 |
| Ba | 855 | 917 | 823 | 929 | 815 | 742 | 596 | 824 | 758 | 781 | 251 | 485 | 348 | 557 | 692 | 717 |
| Zr | 304 | 320 | 267 | 326 | 226 | 204 | 86 | 243 | 206 | 242 | 163 | 259 | 268 | 382 | 250 | 152 |
| Nb | 21 | 20.3 | 20.5 | 21.6 | 10.5 | 10.6 | 3.5 | 7.1 | 5.5 | 7.5 | 22.3 | 26.1 | 8.4 | 11.7 | 14.0 | 7.1 |
| Y | 29.9 | 29.9 | 27.7 | 31.9 | 22 | 22.1 | 7.2 | 17.9 | 15.7 | 17.4 | 11.1 | 15.5 | 34.4 | 48 | 23.6 | 17.3 |
| Ga | 20.5 | 21.1 | 20.1 | 20.5 | 19.5 | 19.3 | 16.5 | 23 | 23 | 21.4 | 20 | 22.3 | 18.8 | 18.5 | 20.3 | – |
| Th | 11.3 | 8.9 | 10.2 | 9.1 | 4.1 | 4.8 | 4.4 | 1.1 | – | 2 | 6.6 | 9.7 | 2.1 | 2.6 | 5.9 | 6.1 |
| U | 5.1 | 4 | 4.6 | 3.9 | 4.9 | 3.2 | 2.8 | 4.9 | 5.6 | 5.2 | 2.2 | 3.5 | 2.8 | 1.6 | 3.9 | 2.1 |

**Table 2.** Rare earth element composition (in ppm) of representative TTG samples from the Fannani Igneous Complex (Egypt). Rock types based on the IUGS classification are granodiorite (GRD) and quartz monzodiorite (QMD)

| Rock sample no. | GRD F-09 | GRD F-20 | GRD F-22 | QMD F-26 | GRD F-28 | FIC average | TTG average |
|---|---|---|---|---|---|---|---|
| La | 40.9 | 29.7 | 14.2 | 17.5 | 24.2 | 25.30 | 26 |
| Ce | 84.8 | 66.2 | 29.2 | 39.6 | 40.5 | 52.06 | 45 |
| Pr | 10.0 | 8.09 | 3.10 | 5.28 | 4.38 | 6.17 | – |
| Nd | 36 | 28.8 | 9.79 | 20.1 | 14 | 21.74 | 18 |
| Sm | 7.86 | 6.2 | 1.85 | 4.67 | 2.66 | 4.65 | 3.5 |
| Eu | 1.75 | 1.54 | 0.79 | 1.69 | 1.03 | 1.36 | 0.95 |
| Gd | 6.28 | 4.85 | 1.32 | 3.71 | 2.11 | 3.65 | 3.0 |
| Tb | 0.94 | 0.71 | 0.19 | 0.51 | 0.36 | 0.54 | 0.49 |
| Dy | 5.28 | 3.95 | 1.04 | 2.76 | 2.11 | 3.03 | – |
| Ho | 1.02 | 0.77 | 0.20 | 0.52 | 0.39 | 0.58 | – |
| Er | 2.93 | 2.33 | 0.61 | 1.45 | 1.05 | 1.67 | – |
| Tm | 0.427 | 0.344 | 0.094 | 0.203 | 0.151 | 0.24 | – |
| Yb | 2.69 | 2.16 | 0.64 | 1.25 | 1.00 | 1.55 | 1.33 |
| Lu | 0.401 | 0.325 | 0.102 | 0.182 | 0.161 | 0.23 | 0.23 |
| ΣREE | 201 | 156 | 63 | 99 | 94 | 123 | – |
| Hf | 9.2 | 6.7 | 3.0 | 5.8 | 5.8 | 6.10 | 4.3 |
| Ta | 1.63 | 0.99 | 0.28 | 0.43 | 2.09 | 1.08 | 0.72 |
| $(La)_N$ | 59.53 | 43.23 | 20.67 | 25.47 | 35.23 | 36.83 | – |
| $(Yb)_N$ | 5.46 | 4.38 | 1.30 | 2.54 | 2.03 | 3.14 | – |
| $(La/Yb)_N$ | 10.91 | 9.87 | 15.92 | 10.05 | 17.37 | 12.82 | 14.2 |

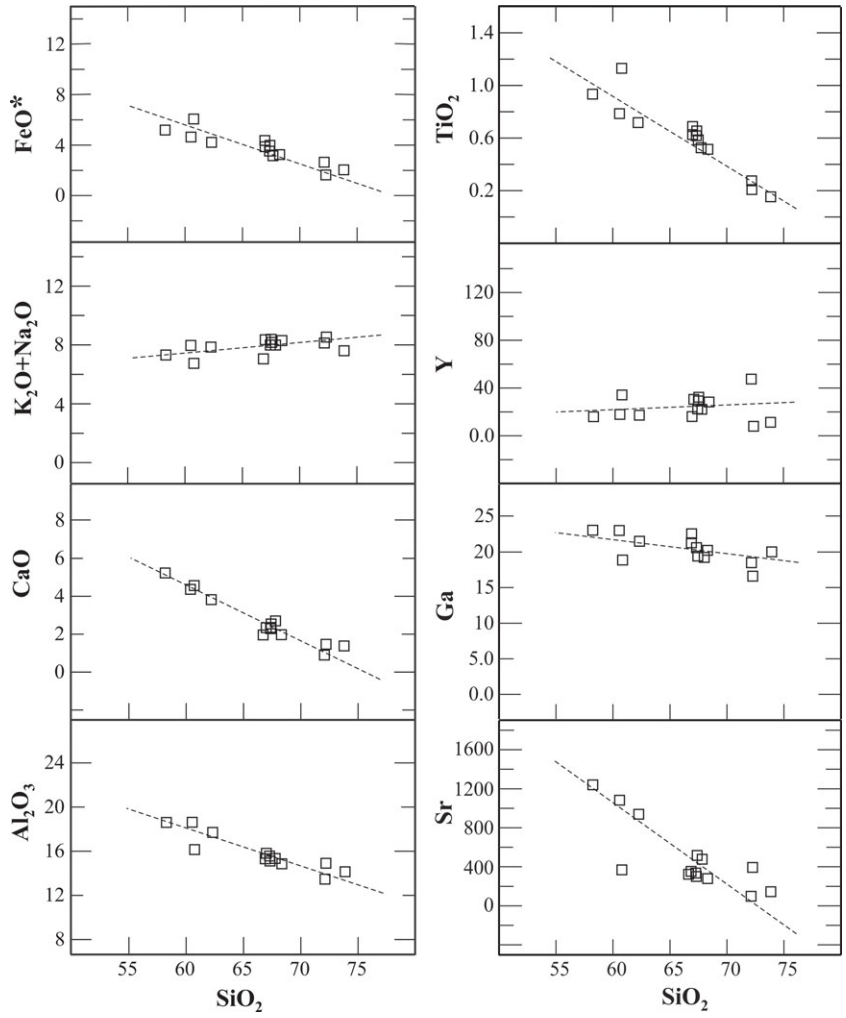


**Fig. 4.** Variations of selected major and trace elements versus silica for rocks of the Fannani complex. Most data points show linear well-defined trends (with some limited scatter), suggesting a continuous process of evolution via internal differentiation.

https://doi.org/10.1017/S0016756820000795 Published online by Cambridge University Press

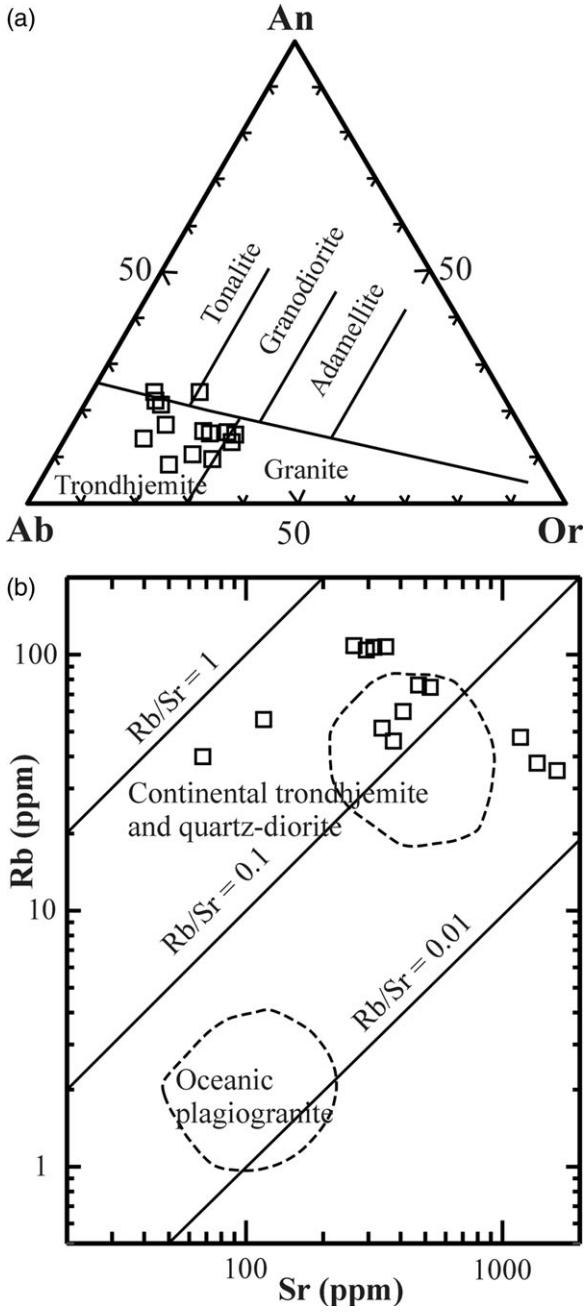


**Fig. 5.** (a) Normative An–Ab–Or classification diagram for the FIC, showing that it is made up of tonalite–trondhjemite–granodiorite (TTG) lithologies; fields are after O'Connor (1965) and Barker (1979). (b) The Rb versus Sr variation diagram indicating that the FIC rocks plot within or near the field of quartz-diorite and continental trondhjemite, and are clearly distinct from oceanic plagiogranites (fields are after Coleman & Peterman, 1975).

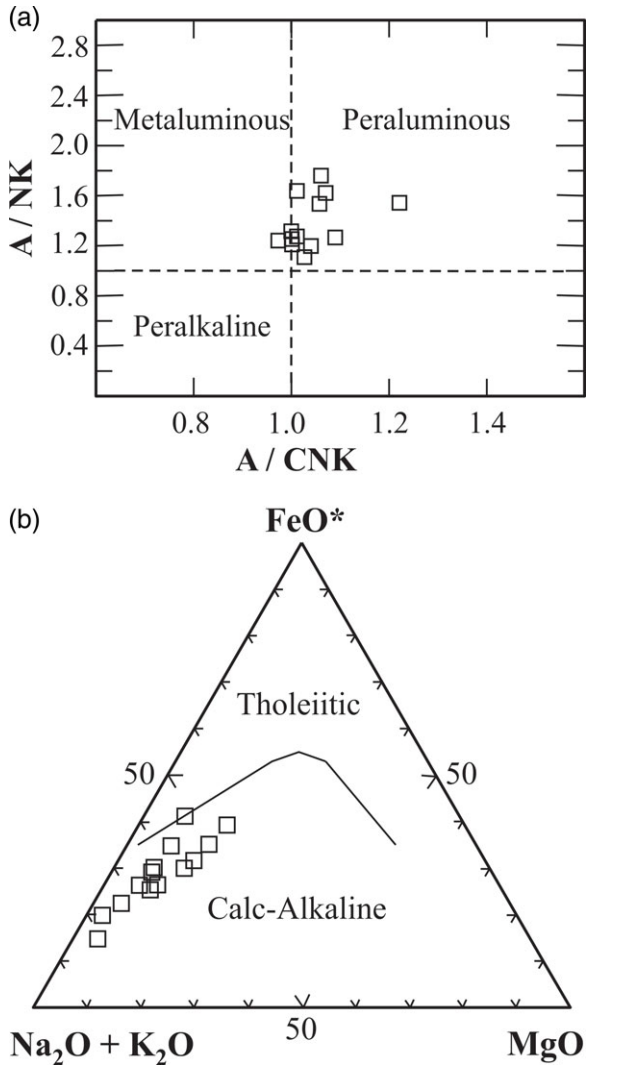


**Fig. 6.** (a) Molecular $Al_2O_3/(CaO + Na_2O + K_2O)$ versus molecular $Al_2O_3/(Na_2O + K_2O)$ (or molar A/CNK versus A/NK) variation diagram showing that the Fannani rocks are predominantly peraluminous in nature. (b) A–F–M diagram showing that lithologies of the Fannani complex exhibit a well-defined calc-alkaline trend.

suggested that chemical traits of the low-HREE group of TTGs generally indicate high-pressure melting conditions. Halla *et al.* (2009) concluded that melting in the lower part of a thick basaltic oceanic crust could produce TTGs of the low-HREE type.

## 5.c. Age of crystallization and isotopic characteristics

### 5.c.1. U–Pb zircon radiometric isotopes

The TIMS method was used for the U–Pb zircon radiometric age dating of the FIC; analytical results are given in Table 3, with uncertainties quoted at the 2$\sigma$ level. The three zircon fractions used for analysis are composed of single grains, and the zircon crystals are all colourless, transparent elongate prisms with well-formed tetragonal dipyramidal terminations. The data are plotted on a Concordia diagram (Fig. 10a). The three zircon grains analysed (Z-1, Z-3 and Z-5) are very slightly discordant and produced $^{206}Pb/^{238}U$ TIMS ages of 607.5 ± 1.21 Ma, 607.4 ± 0.53 Ma and 607.4 ± 1.44 Ma, respectively (Table 3). A precise $^{206}Pb/^{238}U$ mean age of 607.4 ± 1.95 Ma (mean square weighted deviation or MSWD = 0.038) has been obtained on these three zircon grains (Fig. 10a; Table 3), and is considered the age of crystallization of the FIC. The very slightly discordant ages obtained on the zircon grains analysed probably reflect some minor Pb-loss, rather than the time of magma emplacement. An earlier geochronological investigation on rocks that host the FIC (the Meatiq orthogneiss and surrounding rock formations) was carried out by Andresen *et al.* (2009). Their work included a rock sample from the Fannani TTG suite (which they referred to as syn-tectonic diorite), and obtained U–Pb zircon crystallization ages of 609.0 ± 1.0 Ma and 605.8 ± 0.9 Ma. The age determined in the present study

https://doi.org/10.1017/S0016756820000795 Published online by Cambridge University Press

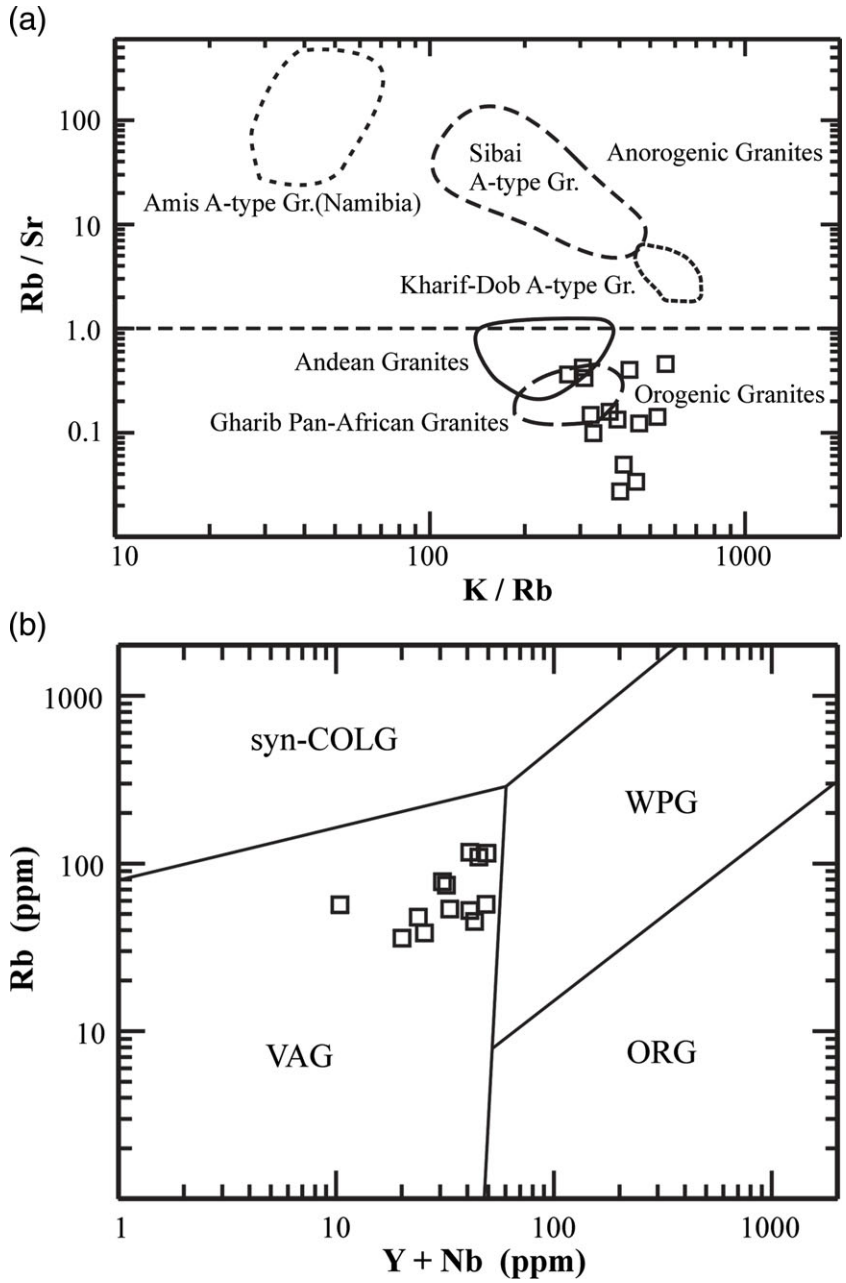


**Fig. 7.** (a) K/Rb versus Rb/Sr diagram showing that all data points of the FIC exhibit very low (< 0.6) Rb/Sr ratios, characteristic of orogenic complexes. The boundary (marked by the dashed line at Rb/Sr = 1) separating the fields of orogenic and anorogenic granites is after Abdel-Rahman & El-Kibbi (2001). The fields of the anorogenic peralkaline granites of the Amis complex of Namibia, of the Sibae complex and the Kharif-Dob complex of eastern Egypt are after Schmitt *et al.* (2000), Abdel-Rahman & El-Kibbi (2001) and Abdel-Rahman (2006), respectively. The fields of the orogenic Andean granites and the Pan-African calc-alkaline granites are after Atherton *et al.* (1979) and Abdel-Rahman & Martin (1987), respectively. (b) Rb versus (Y + Nb) diagram showing that the FIC rocks plot in the field of volcanic-arc granites (VAG). Other fields are collisional granites (COLG), within-plate granites (WPG) and oceanic-ridge granites (ORG), and are after Pearce *et al.* (1984).

(607.4 ± 1.95 Ma) is nearly identical to the middle of the age range obtained by those authors.

It should be noted that TTGs of ages within the Ediacaran period (*c.* 635–541 Ma), such as that of the FIC, are extremely rare in Earth; the FIC example provided here indicates further that TTGs are not strictly an Archean phenomenon, but rather extend to much younger geological times. In fact, Archean and Early Proterozoic cratons occurring within various continents worldwide are dominated by TTG lithologies; their presence in Neoproterozoic shields is uncommon, however, which adds to the significance of this study in contributing to knowledge of Neoproterozoic crustal development. Furthermore, the presence of such a young TTG suite (607.4 Ma) has significant implications for the understanding of shield evolution within the northern-most segment of the ANS, in the context of Ediacaran geodynamic regime and the regional tectonic framework along the EAO (see Discussion, Section 6).

### *5.c.2. Sm–Nd and Rb–Sr whole-rock isotopic characteristics*

Analytical results of neodymium and strontium isotopes of five representative whole-rock samples from the FIC are given in Table 4. Reported also in Table 4 are the initial isotopic ratios

https://doi.org/10.1017/S0016756820000795 Published online by Cambridge University Press

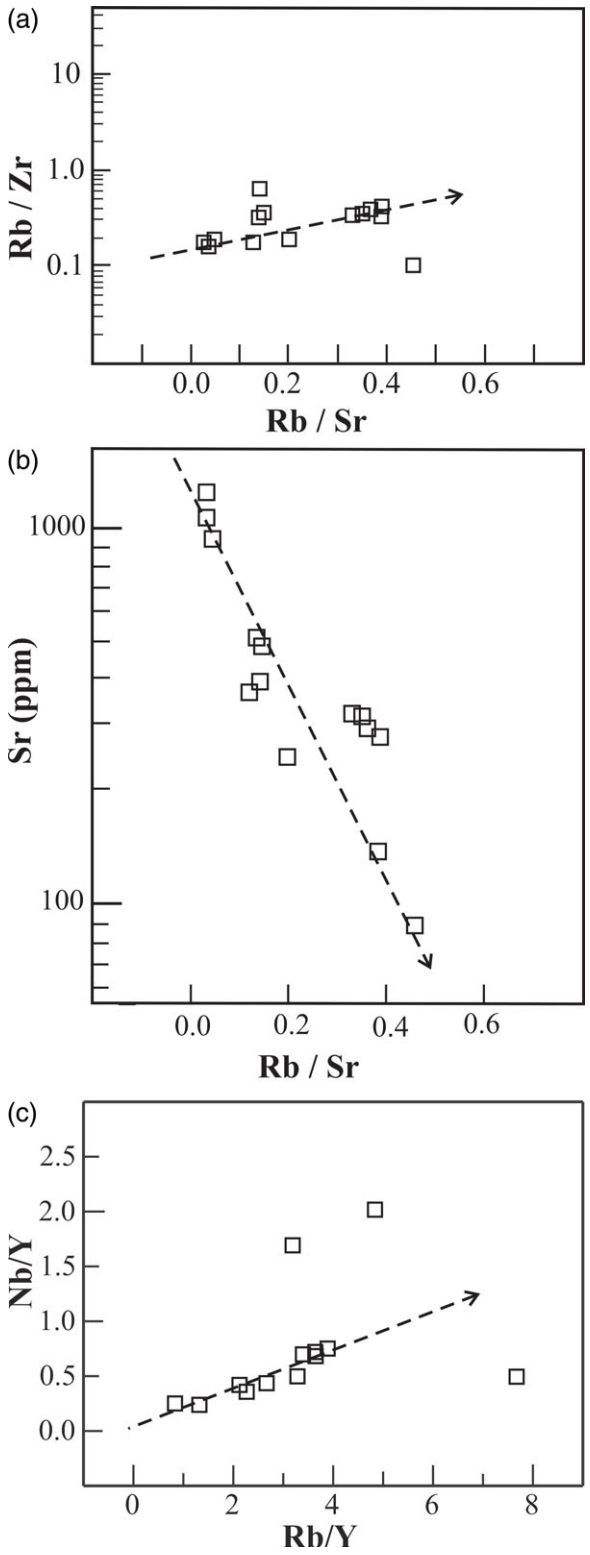


**Fig. 8.** Inter-element variation diagrams of (a) Rb/Sr versus Rb/Zr, (b) Rb/Sr versus Sr and (c) Rb/Y versus Nb/Y for the FIC rocks (see text for details).

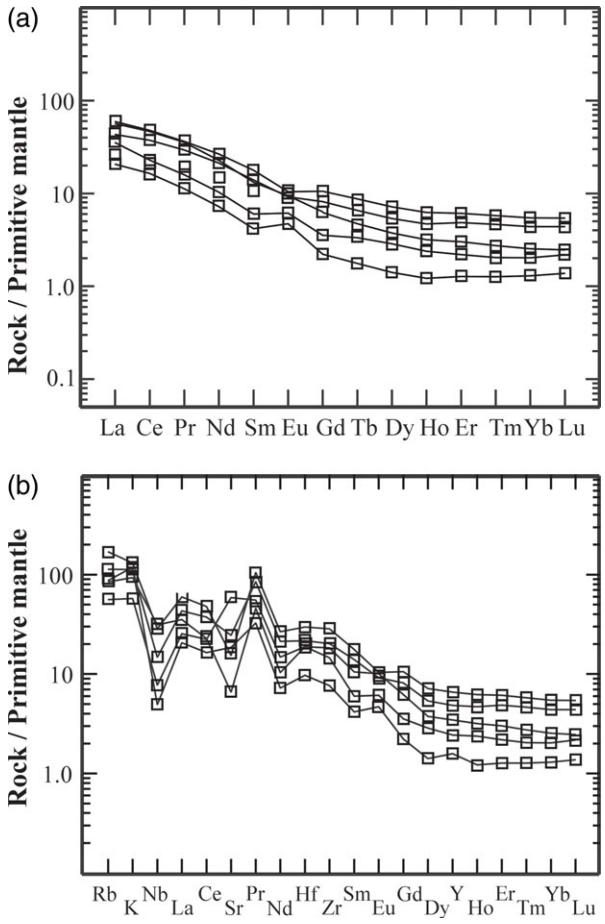


**Fig. 9.** (a) Primitive-mantle-normalized REE patterns of representative samples from the FIC, showing profiles that lack Eu anomalies and exhibit non-fractionated or flat HREEs. (b) Primitive-mantle-normalized multi-element profiles (or spidergram), showing marked depletion in Nb and Sr. Normalization values are taken from Sun & McDonough (1989).

and epsilon values for both Nd and Sr. These initial isotopic ratios $(^{143}Nd/^{144}Nd)_{(i)}$ and $(^{87}Sr/^{86}Sr)_{(i)}$, as well as values of $\epsilon_{Nd}(t)$ and $\epsilon_{Sr}(t)$ for the FIC, have been recalculated to the age of its magma emplacement (607.4 Ma) determined in this study. The decay constants used for these recalculations are those recommended by the IUGS: $^{147}Sm/^{143}Nd = 6.54\times10^{-12}$ $a^{-1}$ (Lugmair & Marti, 1978) and $^{87}Rb/^{87}Sr = 1.42\times10^{-11}$ $a^{-1}$ (Steiger & Jäger, 1977). The values of $\epsilon_{Nd}(t)$ and of $\epsilon_{Sr}(t)$ for the analysed FIC samples are recalculated relative to CHUR with present-day $^{147}Sm/^{144}Nd = 0.1967$, $^{143}Nd/^{144}Nd = 0.512638$ and with present-day $^{87}Rb/^{86}Sr = 0.0736$, $^{87}Sr/^{86}Sr = 0.70391$ (Allégre *et al.* 1983; Faure, 1986).

The Fannani rocks exhibit measured $^{143}Nd/^{144}Nd$ isotopic compositions ranging from 0.512536 to 0.512696, with age-corrected $\epsilon_{Nd}(t)$ values ranging from +5.12 to +7.16. Such high positive initial $\epsilon_{Nd}(t)$ values reflect Pan-African juvenile (mantle-derived) magmatism. The FIC rocks also exhibit measured $^{87}Sr/^{86}Sr$ isotopic compositions ranging from 0.703464 to 0.710911, with age-corrected $^{87}Sr/^{86}Sr_{(i)}$ ratios ranging from 0.70263 to 0.70283 (Table 4). The regression line deduced from whole-rock Rb–Sr isotopic data yields an initial $^{87}Sr/^{86}Sr$ ratio of 0.70284 ± 0.00024 for the FIC rocks. As shown in the $^{87}Sr/^{86}Sr_{(i)}$ versus $\epsilon_{Nd}(t)$ standard diagram (Fig. 10b), the isotopic compositions of the FIC do fall along the mantle array and are clustered within the field of ocean-arc basalts of the Japan-arc, near the MORB field. The Nd–Sr isotopic data of the FIC are therefore similar to those of ocean-arc mafic lavas. This, along with

https://doi.org/10.1017/S0016756820000795 Published online by Cambridge University Press

**Table 3.** Results of U–Pb isotopic analysis (TIMS method) of zircon from the FIC (Egypt) for sample F-27

| | | | | Isotopic ratios | | | | | | | | Age (Ma) | | | | | |
|---|---|---|---|---|---|---|---|---|---|---|---|---|---|---|---|---|---|
| Sample[a] | Th/U | $Pb_c$ (pg)[b] | Pb*/$Pb_c$ | $^{206}Pb/^{204}Pb^c$ | $^{208}Pb/^{206}Pb^d$ | $^{206}Pb/^{238}U^e$ | % Error[f] | $^{207}Pb/^{235}U^e$ | % Error[f] | $^{207}Pb/^{206}Pb^e$ | % Error[f] | Correction coefficient | $^{206}Pb/^{238}U^g$ | ±[h] | $^{207}Pb/^{235}U^g$ | ±[h] | $^{207}Pb/^{206}Pb^g$ | ±[h] |
| Z1 | 0.56 | 0.70 | 7.2 | 441 | 0.176 | 0.098828 | (0.20) | 0.820960 | (1.45) | 0.060250 | (1.35) | 0.550 | 607.50 | 1.21 | 608.58 | 8.80 | 612.5 | 8.3 |
| Z3 | 0.46 | 0.60 | 19.3 | 1182 | 0.144 | 0.098797 | (0.09) | 0.820600 | (0.54) | 0.060240 | (0.51) | 0.500 | 607.40 | 0.53 | 608.35 | 3.31 | 612.2 | 3.1 |
| Z5 | 0.44 | 0.60 | 6.5 | 410 | 0.139 | 0.098801 | (0.24) | 0.821260 | (1.61) | 0.060290 | (1.50) | 0.524 | 607.40 | 1.44 | 608.75 | 9.82 | 613.8 | 9.2 |

[a]Zircon fractions are composed of single grains that are thermally annealed and pre-treated.
[b]Total weight of common Pb in analyses.
[c]Measured ratio corrected for spike and fractionation only.
[d]Radiogenic Pb.
[e]Corrected for fractionation, spike, blank and initial common Pb.
[f]Errors are 2-sigma.
[g]Age calculations are based on the decay constants of Steiger & Jäger (1977).
Mass fractionation correction of 0.25%/amu ± 0.04%/amu (atomic mass unit) was applied to single-collector daily analyses.
Total procedural blank < 0.5 pg for Pb and < 0.1 pg for U.
[h]Error in the dates reported at 2 sigma.
Blank isotopic composition: $^{206}Pb/^{204}Pb = 18.31 \pm 0.53$, $^{207}Pb/^{204}Pb = 15.38 \pm 0.35$, $^{208}Pb/^{204}Pb = 37.45 \pm 1.1$.
Common-Pb corrections were calculated using the model of Stacey & Kramers (1975) and the interpreted age of the sample.

the low initial $^{87}Sr/^{86}Sr$ ratio (0.70284), is suggestive of a mantle-derived source with no or only insignificant contribution from an older continental component (see petrogenesis in Section 6.c).

## 6. Discussion

### 6.a. Tectonic implications for the FIC: did active oceanic subduction extend beyond 620 Ma?

It is well-established that the ANS is composed of a series of juvenile island-arc terranes and developed as a result of the Mozambique Ocean closure (leading to the assembly of Gondwana at *c.* 850–540 Ma; Meert & Torsvik, 2003; Tohver *et al.* 2006) during a long period of island-arc and microcontinent accretion (e.g. Johnson *et al.* 2011; Fritz *et al.* 2013; Robinson *et al.* 2014, 2015). Under question is the timing of cessation of the oceanic-arc late orogenic phase of the EAO and the initiation of a post-collisional and/or extensional regime in northern ANS. While some authors claim that oceanic-arc tectonomagmatic regimes continued to be active until *c.* 650–620 Ma, after which time post-collisional magmatism began, others suggested that subduction orogenic activities and associated arc-magmatism extended beyond 620 Ma. Studies supporting the view that cessation of the oceanic-arc regime occurred at *c.* 620 Ma include those of Eyal *et al.* (2010, 2014, 2019), Be'eri-Shlevin *et al.* (2011), Fritz *et al.* (2013), Jarrar *et al.* (2013) and Elisha *et al.* (2017, 2019). In contrast, a number of other investigations indicated that active subduction extended beyond 620 Ma (Bentor, 1985; Vail, 1990; Küster & Harms, 1998; Teklay *et al.* 2002*a*; Doebrich *et al.* 2007; Bea *et al.* 2009; Andresen *et al.* 2010; Johnson *et al.* 2011; Abu El–Enen & Whitehouse, 2013; Fritz *et al.* 2014; Robinson *et al.* 2014). The later authors stated that the final stages of Gondwana assembly (*c.* 570–530 Ma) are recorded in the northern EAO and are split into two orogenic episodes. The results of this study represent significant contributions to this highly debatable issue, as explained in the following.

#### 6.a.1. Tectonomagmatic implications of the TTG suite of the FIC

It is very clear that the timing of the cessation of subduction and initiation of a post-collisional and/or extensional regime in northern ANS is far from certain. The discovery of this rare Ediacaran TTG suite of the FIC can be used to shed light on this controversial issue. Results of this study show that the high-Al TTG rocks of the FIC form a typical I-type subsolvus suite, of clearly orogenic calc-alkaline affinities with its data points falling exclusively in the field of volcanic-arc granites (Figs 6, 7), and exhibits traits typical of those of I-type, arc-related magmatism. Moreover, the low initial $^{87}Sr/^{86}Sr$ ratio (0.70284) of the FIC, its $\epsilon_{Nd}(t)$ values (+5.12 to +7.16) that fall along the mantle array within the field of Japan-arc basalts (Fig. 10b) and are suggestive of a juvenile magma, along with the progression from intermediate to felsic calc-alkaline lithologies ($SiO_2$ range of 58–74 wt%), are all consistent with an arc setting. The Neoproterozoic island-arc terranes of NE Africa, encompassing several ophiolitic sutures and numerous magmatic complexes (including the FIC), were developed and incorporated into the ANS during various stages of the EAO, and through collisional events during the closure of the Mozambique Ocean (Fig. 11), which ultimately resulted in the collision of East and West Gondwana (*c.* 870–520 Ma; Shackleton, 1996; Wilson *et al.* 1997). Slab melts accompanying

https://doi.org/10.1017/S0016756820000795 Published online by Cambridge University Press

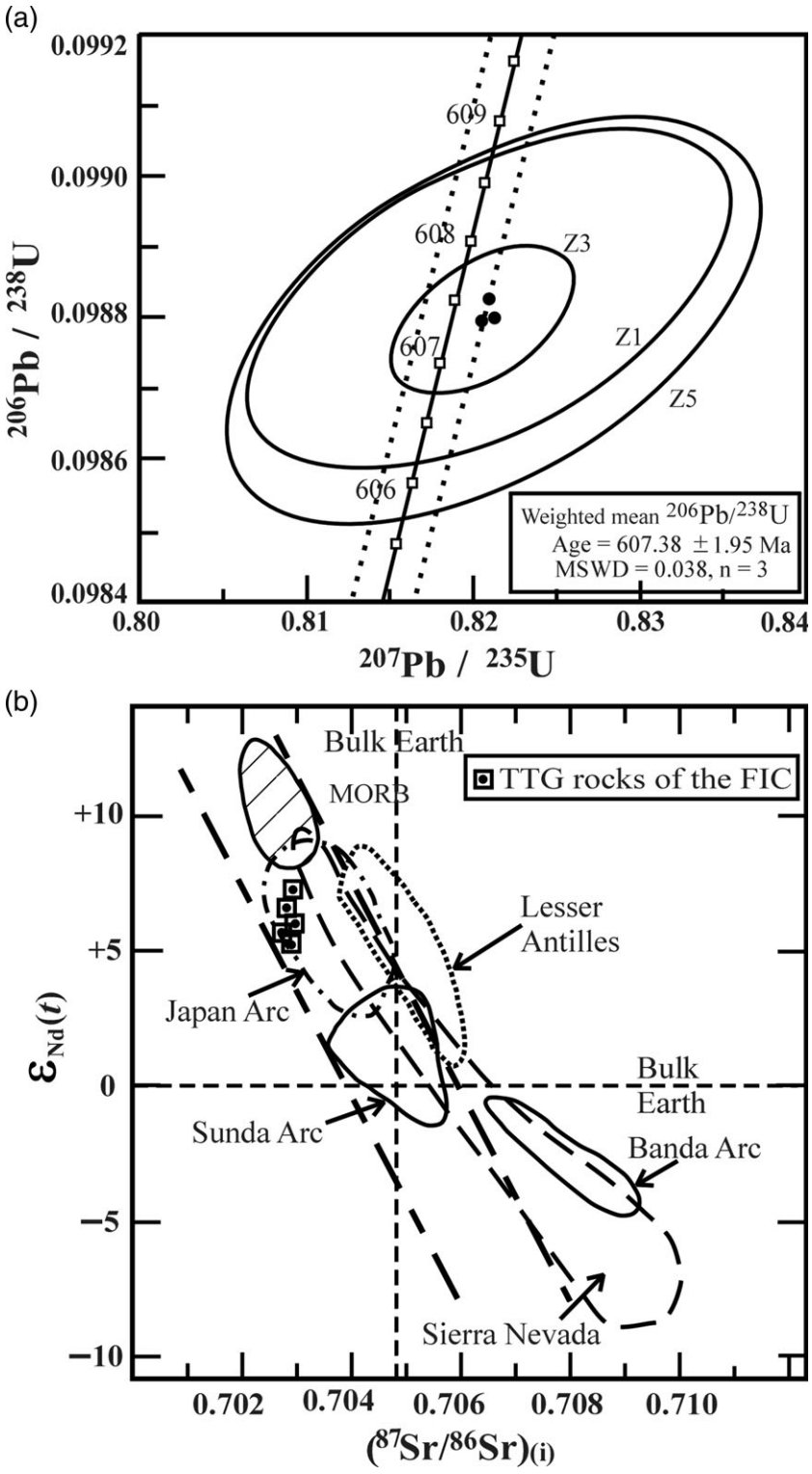


**Fig. 10.** (a) U–Pb concordia diagram for the FIC. Raw data are given in Table 3 (see text for details). (b) Initial Sr ratios ($^{87}Sr/^{86}Sr_{(i)}$) versus $\epsilon_{Nd}(t)$ diagram for representative TTG rocks of the FIC (squares). These initial Sr ratios and $\epsilon_{Nd}(t)$ values have been recalculated to the FIC crystallization age (607.4 Ma) and are given in Table 4. Also plotted in this diagram are some general ranges of values of several types of rock suites from selected tectonic settings: MORB, Japan arc, Lesser Antilles, Sunda Arc, Banda Arc and Sierra Nevada batholith (California). Data for these suites are taken from Faure (1986).

ocean closure, possibly of a subducted Mozambique oceanic crust, may have generated Neoproterozoic TTG magmas such as those of the FIC and many similar magmatic complexes, contributing to welding and consolidating a united (East and West) Gondwana via various stages of the EAO. The Ediacaran age obtained in this study for the TTG suite of the FIC (607.4 Ma) places it within the late orogenic stage that witnessed the closure of the Mozambique Ocean, suggesting that oceanic subduction extended to, and was still operative through, the very late stages of the East African Orogeny. Accordingly, this rare Ediacaran TTG suite of the FIC

https://doi.org/10.1017/S0016756820000795 Published online by Cambridge University Press

**Table 4.** Results of Nd and Sr isotopic analyses of representative TTG samples from the Fannani Igneous Complex (Egypt). Initial isotopic values ($\epsilon_{Nd}(t)$, $\epsilon_{Sr}(t)$) are recalculated relative to CHUR with present-day $^{147}Sm/^{144}Nd = 0.1967$, $^{143}Nd/^{144}Nd = 0.512638$, $^{87}Rb/^{86}Sr = 0.0736$ and $^{87}Sr/^{86}Sr = 0.70391$ (Allégre et al. 1983; Faure, 1986). These values, along with initial ratios ($^{143}Nd/^{144}Nd_{(i)}$, $^{87}Sr/^{86}Sr_{(i)}$), have been recalculated to the FIC crystallization age (607.4 Ma) determined in this study. Decay constants used for these recalculations (recommended by the IUGS) are: $^{87}Rb/^{87}Sr = 1.42\times10^{-11}$ $a^{-1}$ (Steiger & Jäger, 1977) and $^{147}Sm/^{143}Nd = 6.54\times10^{-12}$ $a^{-1}$ (Lugmair & Marti, 1978)

| Sample number | Sm (ppm) | Nd (ppm) | $^{147}Sm/^{144}Nd$ | $^{143}Nd/^{144}Nd$ | Error (2$\sigma$) | $^{143}Nd/^{144}Nd_{(i)}$ | $\epsilon_{Nd}(t)$ (Zr age) |
|---|---|---|---|---|---|---|---|
| F-09 | 8.20 | 40.1 | 0.1236 | 0.512632 | 0.000005 | 0.512141 | +5.554 |
| F-20 | 6.09 | 31.7 | 0.1163 | 0.512647 | 0.000002 | 0.512185 | +6.414 |
| F-22 | 1.96 | 11.3 | 0.1051 | 0.512536 | 0.000003 | 0.512119 | +5.115 |
| F-26 | 4.80 | 23.0 | 0.1263 | 0.512655 | 0.000004 | 0.512154 | +5.795 |
| F-27 | 4.55 | 23.1 | 0.1190 | 0.512696 | 0.000003 | 0.512224 | +7.162 |
| Sample number | Rb (ppm) | Sr (ppm) | $^{87}Rb/^{86}Sr$ | $^{87}Sr/^{86}Sr$ | Error (2$\sigma$) | $^{87}Sr/^{86}Sr_{(i)}$ | $\epsilon_{Sr}(t)$ (Zr age) |
| F-09 | 110 | 332 | 0.9560 | 0.710911 | 0.000006 | 0.702630 | –9.13 |
| F-20 | 72.5 | 530 | 0.3957 | 0.706203 | 0.000004 | 0.702775 | –7.07 |
| F-22 | 55.2 | 402 | 0.3973 | 0.706151 | 0.000003 | 0.702709 | –8.01 |
| F-26 | 32.5 | 1248 | 0.0752 | 0.703464 | 0.000003 | 0.702813 | –6.53 |
| F-27 | 43.3 | 940 | 0.1333 | 0.703982 | 0.000003 | 0.702827 | –6.33 |

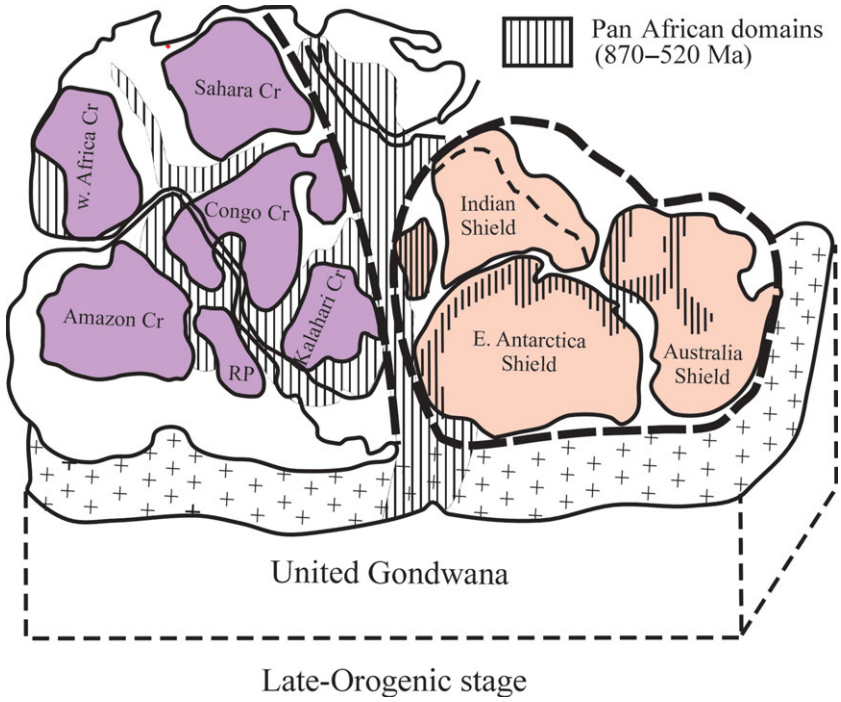


**Fig. 11.** (Colour online) Block diagram showing the closure of the Mozambique Ocean during the late orogenic stage that generated some tonalitic magmas, producing the FIC and similar Pan-African igneous complexes that contributed to the final amalgamation of Gondwana (modified from Meert & Lieberman, 2008).

provides powerful evidence for tracking subduction in the northern segment of the ANS.

### *6.b. Source characteristics, pressure, temperature and melting conditions*

Chemical and isotopic data show that rocks of the FIC belong to the high-Al low-HREE TTG group, represent a volcanic-arc orogenic suite of a peraluminous calc-alkaline nature, and exhibit traits showing strong arc-geochemical signatures that are suggestive of a mafic source (a subducted basaltic oceanic crust). Numerous studies have consistently indicated that TTG magmas are essentially produced by partial melting of eclogite or garnet amphibolite, having a precursor of a subducted basaltic oceanic crust (Rapp, 1994; Rollinson, 1997; Condie, 2005; Halla *et al.* 2009; Almeida *et al.* 2011, 2017). As demonstrated by several authors, trace elements such as Sr, Y, Nb, Ta and the REEs are sensitive to the mineral assemblage of the source rock (e.g. Rapp *et al.* 2003; Xiong *et al.* 2005; Moyen & Stevens, 2006; Moyen, 2009; Almeida *et al.* 2017). For example, Foley *et al.* (2002,

https://doi.org/10.1017/S0016756820000795 Published online by Cambridge University Press

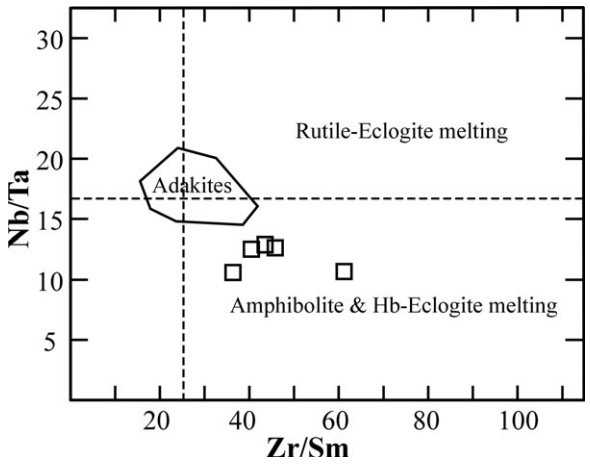


**Fig. 12.** The Nb/Ta versus Zr/Sm diagram of Condie (2005) showing the adakite field in relation to compositional fields representing melting of both rutile eclogite and rutile-free eclogite. Rock samples of the FIC plot away from the adakite field. It should be noted that these rocks plot mainly in the melting field of rutile-free eclogite (see Section 6, Discussion). The melting fields are from Foley *et al.* (2002), and the dashed lines represent primitive mantle values of Sun & McDonough (1989).

2004) and Schmidt *et al.* (2004) showed that partial melting of rutile-bearing eclogite produces liquids with high Nb/Ta ratios (> 16.7 value of primitive mantle; Condie, 2005). However, TTG assemblages exhibit low Nb/Ta ratios. Using data from Martin (1999), Condie (2005) argued that depletion in HREE and the low Nb/Ta ratios (5–15; average, 11) in high-Al TTGs require both garnet and low-Mg amphibole in the restite, indicating melting in the Hb-eclogite stability field at depths of 40–80 km (i.e. $P = 16–26$ kbar), with a temperature range of 700–800°C.

Rocks of the FIC do exhibit low Nb/Ta ratios (in the range 10.6–12.8; average, 11.8) that fall well below primitive mantle values (i.e. < 16.7), and are similar to the average of Proterozoic TTGs in general (average, 9.9; Condie, 2005). On the Nb/Ta versus Zr/Sm variation diagram, the FIC rocks, which represent a high-Al TTG suite, plot away from the 'adakite' field (Fig. 12), implying a mantle source that lacks rutile. This is consistent with the study of Foley *et al.* (2002) that showed that rutile-bearing eclogites cannot serve as sources for most TTG magmas. The Fannani TTG rocks also exhibit low Mg no. (average, 0.39) and low contents of Ni and Sr (average, 17 ppm and 479 ppm, respectively) compared with adakites that possess higher values of Mg no. (> 0.5), Ni (> 20 ppm) and Sr (> 500 and often > 1000 ppm; Condie, 2005). In addition, rocks of the FIC also have relatively high Zr/Sm ratios (in the range 36–61; average, 46) compared with adakites that have an average ratio of less than that of the primitive mantle (i.e. < 25.2). High concentrations of compatible transition elements (such as Mg, Ni and V) in adakites (unlike TTGs; Condie, 2005) are generally ascribed to the interaction of slab melts with the overlying mantle wedge. It should also be noted that interactions between tonalitic melts and mantle peridotites produce 'sanukitoid' magmas enriched in compatible transition elements (Smithies & Champion, 2000; Martin *et al.* 2005). Accordingly, the generation of TTG melts does not involve interaction with the mantle wedge (e.g. Moyen & Stevens, 2006; Almeida *et al.* 2011). This is consistent with the present study, as the low contents of these compatible transition elements (average, 1.2 wt% MgO, 17 ppm Ni, 41 ppm V) in the TTG rocks of the FIC (which are not related to sanukitoid magmas) reflect that there is no geochemical evidence to support interaction between the FIC magma and a mantle wedge.

A possible rutile-free eclogitic source for the TTG suite of the FIC (based on its low Nb/Ta and high Zr/Sm ratios) is indicative of pressures below 15 kbar. In addition, its relatively high Sr contents (average, 479 ppm) as well as Sr/Y ratios (average, 27), along with its REE profiles showing depleted and flat HREEs (Fig. 9), are suggestive of melting in the presence of garnet and amphibole; its melt must have been in equilibrium with garnet. This is also consistent with a *P* range of 10–15 kbar as demonstrated in a number of experimental studies (e.g. Wolf & Wylie, 1994; Rapp & Watson, 1995; Moyen & Stevens, 2006). A rutile-free eclogitic source for the FIC (as inferred above) is indicative of pressures below 15 kbar. In a 10–15 kbar *P* range of melting, plagioclase breaks down, releasing Sr, while Y and Yb would be locked in garnet. The presence of magmatic epidote in the FIC (Fig. 2) suggests a mesozonal crustal level of emplacement with a crystallization pressure of about 5.5 kbar (e.g. Schmidt & Thompson, 1996; Abdel-Rahman, 2016).

Melting temperatures needed to produce liquids of TTG compositions at various pressures as determined experimentally were in the ranges of 750–975°C at $P = 10$ kbar (Wolf & Wyllie, 1989), 700–800°C (Martin, 1999; Condie, 2005), 1100°C at $P = 16–22$ kbar (Rapp *et al.* 1988), and 900–1100°C at $P = 10–25$ kbar (Moyen & Stevens, 2006). Almeida *et al.* (2011) indicated that tonalite liquids are obtained at *c.* 1000°C ($P < 15$ kbar), and require higher temperatures as pressure rises (*c.* 1200°C at 30 kbar), while trondhjemitic liquids are generated at temperatures below 1000°C. Assuming a pressure in the middle of a 10–15 kbar *P* range at the melting site, it is doubtful that such a *P* range corresponding to the stability domain of garnet (necessary to explain the low La/Yb ratio of the Fannani TTG rocks) could have been attained at 700–800°C, and an assumed melting temperature in the 850–950°C range might be more realistic.

### 6.c. Petrogenesis of the Fannani TTG suite

The orogenic calc-alkaline nature of the high-Al TTG suite of the FIC and its strong arc geochemical signatures (having low $K_2O/Na_2O$ ratios (average, 0.61), high Sr/Y ratios (average, 27), large Ba enrichment (average, 692 ppm), strong depletions in $TiO_2$ (average, 0.6 wt%), Nb (average, 14 ppm) and Yb (average, 1.55 ppm)) are consistent with magma produced by typical slab melts. Other studies, including that of Moyen & Stevens (2006) and Moyen & Martin (2012) indicated that tholeiitic basalt seems to be the most appropriate to account for the genesis of most TTGs.

Results of the Nd–Sr isotopes described above (Section 5.c.2) show that TTG rocks of the FIC exhibit relatively high $^{143}Nd/^{144}Nd$ ratios (average, 0.51263), coupled with a very low initial $^{87}Sr/^{86}Sr$ ratio (0.7028). The age-corrected $\epsilon_{Nd}(t)$ values of the FIC that range from +5.12 to +7.16, along with its recalculated initial Sr ratios ($^{87}Sr/^{86}Sr_{(i)} = 0.70263–0.70283$; Table 4), are suggestive of slab melts. These FIC isotopic compositions fall along the mantle array and are clustered in the field of ocean-arc basalts of the Japan arc (Fig. 10b). Moreover, the high positive initial $\epsilon_{Nd}(t)$ values obtained in this study reflect juvenile mantle-derived magmatism, and the remarkably restricted initial values (extending only to 2 $\epsilon_{Nd}(t)$ units; Table 4) support an intra-oceanic origin for the FIC. Such narrow $\epsilon_{Nd}(t)$ ranges have been reported for modern oceanic-arc volcanic rocks, such as those from the Mariana arc (having a spread of 1.9 $\epsilon_{Nd}(t)$ units; Woodhead, 1989)

https://doi.org/10.1017/S0016756820000795 Published online by Cambridge University Press

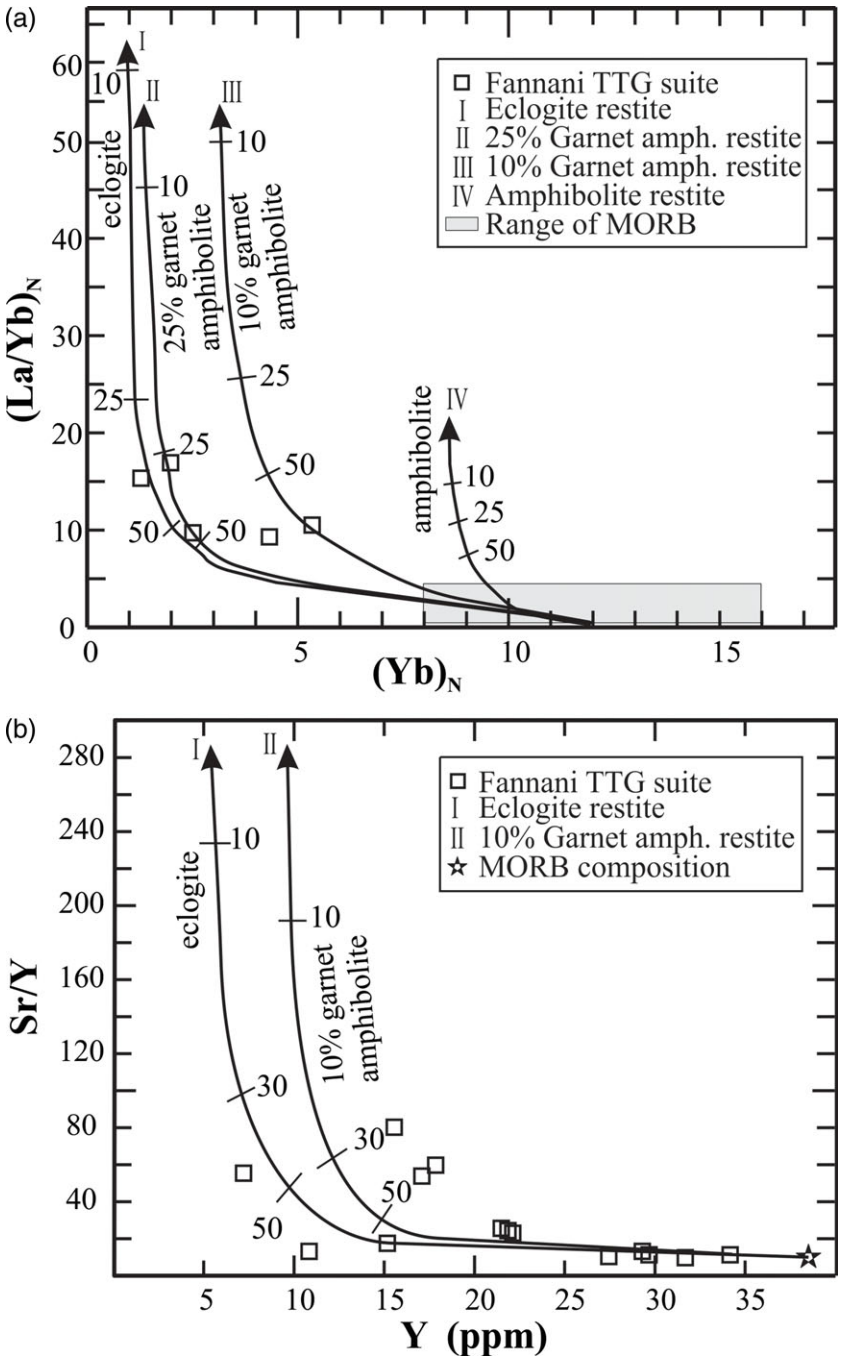


**Fig. 13.** (a) $(Yb)_N$ versus $(La/Yb)_N$ diagram and (b) Y (ppm) versus (Sr/Y) diagram containing various partial melting curves produced using initial MORB source materials (modified after Drummond & Defant, 1990; Martin, 1993) for the Fannani TTG suite. Data points of this suite plot along the garnet-amphibolite and eclogite curves, suggesting its magma was generated by partial melting ($F = 0.25$–$0.50$), leaving eclogitic, or 10–25% garnet-amphibolitic, restite (see text for details).

and from the Kermadec arc (with a spread of 2.7 $\epsilon_{Nd}(t)$ units; Gamble *et al.* 1993), unlike volcanic rocks from modern active continental margins with their much greater $\epsilon_{Nd}(t)$ ranges (e.g. Hawkesworth *et al.* 1993). Furthermore, the FIC possesses even higher $\epsilon_{Nd}(t)$ values than those reported for much older Pan-African assemblages, such as the 854 Ma Eritrean metavolcanics of the southern Nubian Shield ($\epsilon_{Nd}(t)$ of +4.8 to +5.7) that were interpreted by Teklay *et al.* (2002*b*) to have formed in an oceanic-island-arc setting. A mantle source and an oceanic-subduction environment are therefore supported by the chemical and isotopic traits of the TTG rocks of the FIC.

More specifically, Drummond & Defant (1990) and Condie (2005) indicated that partial melting of a basaltic slab under eclogitic and/or garnet-amphibolitic conditions leaving around 10–15% garnet in the residue produces high-Al TTG magma characterized by low (< 1.8 ppm) Yb (it is 1.55 ppm in the FIC), high $(La/Yb)_N$ values (12.8 in FIC), low (< 20 ppm) Y (23.6 ppm in FIC), Nb/Ta values of 7–20 (11.8 in FIC), and high (> 20) Sr/Y and Zr/Sm ratios (27 and 46 in FIC, respectively). The moderately high Kd values of garnet-Hb-Cpx for Y and their low Kd values for Sr allowed the FIC melt to evolve to low Y contents and high Sr/Y ratios. In brief, chemical data of the investigated

https://doi.org/10.1017/S0016756820000795 Published online by Cambridge University Press

TTG suite (with its high-Al and low-HREE nature) suggest a comparable petrogenetic scenario, supporting the inference of slab melting under eclogitic conditions leaving residual garnet in the source. Similarly, a petrogenetic process envisaged by a number of authors (e.g. Drummond & Defant, 1990; Condie, 2005; Martin *et al.* 2005; Moyen & Stevens, 2006; Almeida *et al.* 2011) and that is widely accepted involves anatexis of a basaltic slab under eclogitic conditions leaving garnet in the residue to produce TTG magmas. On the diagram containing various partial melting curves produced from MORB source materials (after Drummond & Defant, 1990; Martin, 1993), data points of the TTG suite of the FIC plot along the eclogite and garnet-amphibolite curves, suggesting its magma was generated by partial melting ($F = 0.25–0.50$) leaving eclogitic- or 10–25% garnet-amphibolitic restite (Fig. 13).

The petrogenetic scenario presented here conforms to the proposal that widespread recycling of the Neoproterozoic oceanic crust must have accompanied the formation of the vast island-arc terranes within the various Pan-African belts, which also host several ophiolitic sutures. The closure of the Mozambique Ocean (Fig. 11) took place via convergence of East and West Gondwana (*c.* 870–520 Ma; Shackleton, 1996; Wilson *et al.* 1997). Slab melts accompanying this closure seem to have produced voluminous orogenic calc-alkaline magmas that were responsible for crustal development in NE Africa and Arabia. In summary, melting of a subducted Mozambique oceanic crust (transformed into eclogite in an oceanic-arc environment) generated TTG magmas that produced the FIC and similar other Neoproterozoic igneous complexes, forming large juvenile belts along the EAO, suturing East and West Gondwana together and assembling them into a united supercontinent during the Neoproterozoic Era.

## 7. Conclusions

(1) The Fannani Igneous Complex was emplaced between low-grade metasedimentary and ophiolitic assemblages to the south, and a high-grade gneissic dome mantled by mylonitic and/or metapelitic schists to the north. Its undeformed, monotonous rocks exhibit magmatic-flow textures, and contain abundant sodic plagioclase and variable contents of quartz, K-feldspar, hornblende, biotite and magmatic epidote, along with accessory titanite, zircon, apatite and rare allanite.

(2) Geochemical data of the FIC indicate that it is a high-Al TTG suite characterized by a wide range of $SiO_2$, $Al_2O_3$, Sr and Zr, has moderate enrichment in REE, depletion in K, Ti, Nb, Y, Hf and HREE, and exhibits moderately fractionated REE profiles, therefore showing clear orogenic affinities and strong arc-geochemical signatures.

(3) Results of the isotopic study show that the FIC exhibits an initial Sr ratio of 0.70284, and age-corrected $\epsilon_{Nd}(t)$ values of +5.1 to +7.2, with Sr–Nd compositions typical of modern oceanic-arc rocks, suggestive of mantle sources and island-arc settings. The precise U–Pb zircon TIMS age obtained (607.4 Ma) indicates that the FIC is a rare Ediacaran TTG suite, and implies its magma generation accompanied the closure of the Mozambique Ocean during the very late stages of the EAO.

(4) The high-Al TTG rocks of the FIC exhibit chemical and isotopic traits indicative of magmas produced by anatexis of a basaltic slab. Partial melting models indicate that the FIC magma was generated via melting ($F = 0.25–0.50$) of a subducted oceanic crust transformed into eclogite, leaving 10–25% garnet in the residue. Thus, melting of a subducted eclogitic Mozambique oceanic crust generated tonalitic magmas that produced the FIC and similar other Neoproterozoic igneous complexes along the EAO, forming large juvenile belts that sutured East and West Gondwana together into a united supercontinent. Accordingly, this rare Ediacaran TTG suite provides powerful evidence for tracking subduction, which must have been operative through the very late stages of the East African Orogeny.

Particularly relevant will be detailed investigations of similar igneous complexes in the region to determine the extent of Ediacaran TTG plutonism occurring within the ANS, and its role in evaluating processes of Neoproterozoic crustal development in NE Africa and Arabia and in comparisons with processes dominated during the earlier phases of crustal evolution during the Archean Eon.

**Acknowledgements.** Dr Z. El-Alfey of the Geological survey of Egypt is thanked for providing facilities during the field investigation. Dr Serge Nadeau is acknowledged for helpful suggestions and a fruitful exchange of ideas during the initial phase of this work. Professor R. F. Martin is thanked for discussions and useful comments. I wish to acknowledge the assistance of Dr Y. Kapusta in performing the radiometric isotopic analyses. I thank both Ms Eliane Shwairi and Mr Maroun Ijreiss of the American University of Beirut for providing some technical assistance. The comments and corrections of reviewers and the editor significantly improved the quality of this manuscript, and are much appreciated. I am grateful to Dr K. Goodenough for careful editing of this contribution. This work was supported by an internal AUB university research grant to the author.

## References

**Abdel-Rahman AM** (1990) Petrogenesis of early-orogenic diorites, tonalities and post-orogenic trondhjemites in the Nubian Shield. *Journal of Petrology* **31**, 1285–312.

**Abdel-Rahman AM** (1995) Tectonic-magmatic stages of shield evolution: the Pan-African belt in northeastern Egypt. *Tectonophysics* **242**, 223–40.

**Abdel-Rahman AM** (1996) Pan African volcanism: petrology and geochemistry of the Dokhan Volcanic Suite in the northern Nubian shield. *Geological Magazine* **133**, 17–31.

**Abdel-Rahman AM** (2006) Petrogenesis of anorogenic peralkaline granitic complexes from eastern Egypt. *Mineralogical Magazine* **70**, 27–50.

**Abdel-Rahman AM** (2010) Nature of feldspars in felsic plutonic complexes from northeastern Egypt: implications for the evolution of orogenic and anorogenic magmas. *Neues Jahrbuch Für Geologie und Paläontologie Abhandlungen* **257**, 147–68.

**Abdel-Rahman AM** (2016) Mineralogy of the Neoproterozoic epidote-bearing TTG suite, Mons Claudianus batholith (Egypt) and implications for synorogenic magmatism. *Mineralogical Magazine* **80**, 1291–314.

**Abdel-Rahman AM** (2019) Geochemistry, age and origin of the Mons Claudianus TTG batholith (Egypt): insight into the role of Pan-African magmatism in uniting plates of Gondwana. *Geological Magazine* **156**, 969–88.

**Abdel-Rahman AM and Doig R** (1987) The Rb-Sr geochronological evolution of the Ras Gharib segment of the northern Nubian shield. *Journal of the Geological Society of London* **144**, 577–86.

**Abdel-Rahman AM and El-Kibbi MM** (2001) Anorogenic magmatism: chemical evolution of the Mount El-Sibai A-type complex (Egypt), and implications for the origin of within-plate felsic magmas. *Geological Magazine* **138**, 67–85.

**Abdel-Rahman AM and Martin RF** (1987) Late Pan-African magmatism and crustal development in northeastern Egypt. *Geological Journal* **22**, 281–301.

**Abdel-Rahman Y, Polat A, Dilek Y, Fryer BJ, El-Sharkawy M and Sakran S** (2009) Geochemistry and tectonic evolution of the Neoproterozoic incipient

https://doi.org/10.1017/S0016756820000795 Published online by Cambridge University Press

arc-forearc crust in the Fawakhir area, Central Eastern Desert, Egypt. *Precambrian Research* **175**, 116–34.

**Abu El-Enen MM and Whitehouse MJ** (2013) The Feiran-Solaf Metamorphic Complex, Sinai, Egypt: geochronological and geochemical constraints on its evolution. *Precambrian Research* **239**, 106–25.

**Akaad MK and Noweir AM** (1969) Lithostratigraphy of the Hammamat - Um Seleimat district, Eastern Desert, Egypt. *Nature* **223**, 284–5.

**Akaad MK and Shazly AG** (1972) Description and petrography of the Meatiq Group. *Annals Geological Survey of Egypt* **2**, 215–38.

**Akaad MK and Shazly AG** (1975) Lithostratigraphy of the Abu Ziran area, Eastern Desert, Egypt. In *Proceedings of the 13th Annual Meeting of the Geological Society of Egypt*, Cairo: Geological Society of Egypt, Abstract 13, pp. 23.

**Ali KA, Azer MK, Gahlan HA, Wilde SA, Samuel MD and Stern RJ** (2010) Age constraints on the formation and emplacement of Neoproterozoic ophiolites along the Allaqi–Heiani Suture, South Eastern Desert of Egypt. *Gondwana Research* **18**, 583–95.

**Allégre CJ, Hart SR and Minster JF** (1983) Chemical structure and evolution of the mantle and continents determined by inversion of Nd and Sr isotope data, II. Numerical experiments and discussion. *Earth Planetary Science Letters* **37**, 191–213.

**Almeida JAC, Dall'Agnol R, Oliveira MA, Macambirab MJB, Pimenteld MM, Rämöe OT, Guimarãesa FV and Leite AAS** (2011) Zircon geochronology, geochemistry and origin of the TTG suites of the Rio Maria granite-greenstone terrane: implications for the growth of the Archean crust of the Carajás province, Brazil. *Precambrian Research* **187**, 201–21.

**Almeida JAC, Dall'Agnol R and Rocha MC** (2017) Tonalite–trondhjemite and leucogranodiorite–granite suites from the Rio Maria domain, Carajas Province, Brazil: implications for discrimination and origin of the Archean Na-granitoids. *Canadian Mineralogist* **55**, 437–56.

**Andresen A, Augland LE, Boghdady GY, Lundmark AM, Elnady OM, Hassan MA and Abu El-Rus MA** (2010) Structural constraints on the evolution of the Meatiq Gneiss Dome (Egypt), East-African Orogen. *Journal of African Earth Sciences* **57**, 413–22.

**Andresen A, El-Rus MMA, Myhre PI, Boghdady GY and Corfu F** (2009) U–Pb TIMS age constraints on the evolution of the Neoproterozoic Meatiq Gneiss Dome, Eastern Desert, Egypt. *International Journal of Earth Sciences* **98**, 481–97.

**Atherton MP, McCourt WJ, Sanderson LM and Taylor WP** (1979) The geochemical character of the segmented Peruvian Coastal batholith and associated volcanics. In *Origin of Granite Batholiths: Geochemical Evidence* (eds MP Atherton and J Tarney), pp. 45–64. Cheshire, UK: Shiva.

**Barker F** (1979) Trondhjemite: definition, environment and hypothesis of origin. In *Trondhjemites, Dacites and Related Rocks* (ed. F Barker), pp. 1–12. Amsterdam: Elsevier.

**Barker F and Arth JG** (1976) Generation of trondhjemitic-tonalitic liquids and Archean bimodal trondhjemite basalt suites. *Geology* **4**, 596–600.

**Barker F, Peterman ZE and Friedman L** (1976) The 1.7 to 1.8 b.y. old trondhjemites of southwestern Colorado and northern New Mexico: geochemistry and depths of genesis. *Geological Society of America Bulletin* **87**, 189–98.

**Barr SM, White CE and Culshaw NG** (2001) Geology and tectonic setting of Paleoproterozoic granitoid suite in the Island Harbour Bay area, Makkovick Province, Labrador. *Canadian Journal of Earth Sciences* **38**, 441–63.

**Bea F, Abu-Anbar M, Montero P, Peres P and Talavera C** (2009) The ~844Ma Moneiga quartz-diorites of the Sinai, Egypt: evidence for Andean-type arc or rift-related magmatism in the Arabian-Nubian Shield? *Precambrian Research* **175**, 161–68.

**Bédard JH** (2003) Evidence for regional-scale, pluton-driven, high-grade metamorphism in the Archean Minto Block, northern Superior Province, Canada. *Journal of Geology* **111**, 183–205.

**Bédard JH** (2006) A catalytic delamination-driven model for coupled genesis of Archaean crust and sub-continental lithospheric mantle. *Geochimica et Cosmochimica Acta* **70**, 1188–214.

**Be'eri-Shlevin Y, Katzir Y and Whitehouse M** (2009) Post-collisional tectono-magmatic evolution in the northern Arabian-Nubian Shield (ANS): time constraints from ion-probe U-Pb dating of zircon. *Journal of Geological Society of London* **166**, 71–85.

**Be'eri-Shlevin Y, Samuel MD, Azer MK, Ramo OT, Whitehouse MJ and Moussa HE** (2011) The Ediacaran Ferani and Rutig volcano-sedimentary successions of the northernmost Arabian-Nubian Shield (ANS): new insights from zircon U–Pb geochronology, geochemistry and O–Nd isotope ratios. *Precambrian Research* **188**, 21–44.

**Bentor YK** (1985) The crustal evolution of the Arabian–Nubian Massif with special reference to the Sinai Peninsula. *Precambrian Research* **28**, 1–74.

**Berhe SM** (1990) Ophiolites in Northeast and East Africa: implications for Proterozoic crustal growth. *Journal of the Geological Society of London* **147**, 41–57.

**Blasband B, White S, Broijmans P, De Boorder H and Visser W** (2000) Late Proterozoic extensional collapse in the Arabian-Nubian shield. *Journal of the Geological Society of London* **157**, 615–28.

**Castillo PR** (2006) An overview of adakite petrogenesis. *Chinese Science Bulletin* **51**, 257–68.

**Castillo PR** (2008) The origin of the adakite – high-Nb basalt association and its implications for post-subduction magmatism in Baja California, Mexico. *Geological Society of America Bulletin* **120**, 451–62.

**Castillo PR** (2012) Adakite petrogenesis. *Lithos* **134–135**, 304–16.

**Church WR** (1988) Ophiolites, sutures, and micro-plates of the Arabian-Nubian Shield: a critical comment. In *The Pan-African Belt of Northeast Africa and Adjacent Areas* (eds S E1 Gaby and RO Greiling), pp. 289–316. Braunschweig/Wiesbaden: Friedrich Vieweg & Sohn.

**Coleman RG and Peterman ZE** (1975) Oceanic plagiogranite. *Journal of Geophysical Research* **80**, 1099–108.

**Condie KC** (1998) Episodic continental growth and supercontinents: a mantle avalanche connection? *Earth and Planetary Science Letters* **163**, 97–108.

**Condie KC** (2005) TTGs and adakites: are they both slab melts? *Lithos*, **80**, 33–44.

**Condon DJ, Schoene B, McLean NM, Bowring SA and Parrish RR** (2015) Metrology and traceability of U–Pb isotope dilution geochronology (EARTHTIME Tracer Calibration Part I). *Geochimica et Cosmochimica Acta* **164**, 464–80.

**Cox GM, Foden J and Collins AS** (2019) Late Neoproterozoic adakitic magmatism of the eastern Arabian Nubian Shield. *Geoscience Frontiers* **10**, 1981–92.

**Dahlquist JA** (2001) REE fractionation by accessory minerals in epidote-bearing metaluminous granitoids from the Sierras Pampeanas, Argentina. *Mineralogical Magazine* **65**, 463–75.

**Defant MJ and Drummond MS** (1990) Derivation of some modern arc magmas by melting of young subducted. *Nature* **367**, 662–5.

**Doebrich JL, Al-Jehani AM, Siddiqui AA, Hayes TS, Wooden JL and Johnson PR** (2007) Geology and metallogeny of the Ar Rayn terrane eastern Arabian shield: evolution of a Neoproterozoic continental-margin arc during assembly of Gondwana within the East African orogen. *Precambrian Research* **158**, 17–50.

**Drummond MS and Defant MJ** (1990) A model for trondhjemite–tonalite–dacite genesis and crustal growth via slab melting: Archaean to modern comparisons. *Journal of Geophysical Research* **95**, 21503–21.

**El-Bialy MZ** (2013) Geochemistry of the Neoproterozoic metasediments formation, Kid metamorphic complex, Sinai, Egypt: implications for source-area weathering, provenance, recycling and depositional tectonic setting. *Lithos* **175**, 68–85.

**El Gaby S** (1976) The Meatiq gneissose granite. In *Proceedings of the 14th Annual Meeting of the Geological Society of Egypt*, Cairo: Geological Society of Egypt, Abstract 14, pp 31.

**El-Gaby S, El-Nady O and Khudeir A** (1984) Tectonic evolution of the basement complex in the Central Eastern Desert of Egypt. *Geologische Rundschau* **73**, 1019–36.

**El-Gaby S, List FK and Tehrani R** (1988) Geology, evolution and metallogenesis of the Pan-African Belt in Egypt. In *The Pan-African Belt of Northeast Africa and Adjacent Areas* (eds S E1 Gaby and RO Greiling), pp. 17–68. Braunschweig/Wiesbaden: Friedrich Vieweg & Sohn.

**El-Gaby S, List FK and Tehrani R** (1990) The basement complex of the Eastern Desert and Sinai. In *The Geology of Egypt* (ed. R Said), pp 175–184. Rotterdam: Balkema.

**Elisha B, Katzir Y, Kylander-Clark A, Golan T and Coble MA** (2019) The timing of migmatization in the northern Arabian–Nubian Shield: evidence

https://doi.org/10.1017/S0016756820000795 Published online by Cambridge University Press

for a juvenile sedimentary component in collision-related batholiths. *Journal of Metamorphic Geology* **37**, 591–610.

**Elisha B, Kylander-Clark A and Katzir Y** (2017) Ediacaran (~620 Ma) high-grade regional metamorphism in the northern Arabian Nubian Shield: U-Th-Pb monazite ages of the Elat schist. *Precambrian Research* **295**, 172–86.

**Eliwa HA, Kimura JI and Itaya T** (2006) Late Neoproterozoic Dokhan Volcanics, North Eastern Desert, Egypt: geochemistry and petrogenesis. *Precambrian Research* **151**, 31–52.

**El-Ramly MF** (1972) A new geological map for the basement rocks in the Eastern and South-Western Desert of Egypt. *Annals of the Geological Survey of Egypt* **2**, 1–18.

**El-Ramly MF, Greiling RO, Kröner A and Rashwan AA** (1984) On the tectonic evolution of the Wadi Hafafit area and environs, Eastern Desert of Egypt. *King Abdulaziz University, Institute of Applied Geology Bulletin* **6**, 113–26.

**El-Sayed MM, Furnes H and Mohamed FH** (1999) Geochemical constraints on the tectonomagmatic evolution of the late Precambrian Fawakhir ophiolite, Central Eastern Desert, Egypt. *Journal of African Earth Sciences* **29**, 515–33.

**El-Sayed MM, Obeid MA, Furnes H and Moghazi AM** (2004) Late Neoproterozoic volcanism in southern Eastern Desert, Egypt: petrological, structural and geochemical constraints on the tectonic-magmatic evolution of the Allaqi Dokhan Volcanic suite. *Neues Jahrbuch Für Mineralogie Abhandlungen* **180**, 261–86.

**El-Shazly SM and El-Sayed MM** (2000) Petrogenesis of the Pan-African El-Bula igneous suite, central Eastern Desert, Egypt. *Journal of African Earth Sciences* **31**, 317–36.

**El-Shazly AG and Essawy MA** (1978) Petrological and geochemical characteristics of the granitic rocks of Abu Ziran district, Eastern Desert, Egypt. In *Proceedings of the 5th Iraqi Geological Congress*, Baghdad: Geological Society of Iraq, Abstract no. 5, pp. 18.

**Evans BW and Vance JA** (1987) Epidote phenocrysts in dacitic dikes, Boulder County, Colorado. *Contributions to Mineralogy and Petrology* **96**, 178–85.

**Eyal M, Be'eri-Shlevin Y, Eyal Y, Whitehouse MJ and Litvinovsky B** (2014) Three successive Proterozoic island arcs in the Northern Arabian-Nubian Shield: evidence from SIMS U-Pb dating of zircon. *Gondwana Research* **25**, 338–57.

**Eyal Y, Eyal M, Litvinovsky B, Jahn B–M, Calvo R and Golan T** (2019) The evolution of the Neoproterozoic Elat Metamorphic Complex, northernmost Arabian-Nubian Shield: Island arc to syncollisional stage and post-collisional magmatism. *Precambrian Research* **320**, 137–70.

**Eyal M, Litvinovsky B, Jahn BM, Zanvilevich A and Katzir Y** (2010) Origin and evolution of post-collisional magmatism: coeval Neoproterozoic calc-alkaline and alkaline suites of the Sinai Peninsula. *Chemical Geology* **269**, 153–79.

**Farrow CEG and Barr SM** (1992) Petrology of high-Al-hornblende and magmatic epidote-bearing plutons in the southeastern Cape Breton Highlands, Nova Scotia. *Canadian Mineralogist* **30**, 377–92.

**Faure G** (1986) *Principles of Isotope Geology*, 2nd ed. New York: John Wiley & Sons, 589 pp.

**Foley SF, Tiepolo M and Vannucci R** (2002) Growth of early continental crust controlled by melting of amphibolite in subduction zones. *Nature* **417**, 837–40.

**Foley SF, Vannucci R, Tiepolo M, Oberti R and Zanetti A** (2004) Recognition of melts of subducted slabs by high field strength element fractionation. In *Proceedings of EGU Meeting*, Nice: European Geophysical Union, April 2004.

**Franz G and Smelik EA** (1995) Zoned zoisite from Weissenstein pegmatite that derived from high-pressure melting of eclogite at ≈ 2.0 GPa: importance for decompressional melting in Eclogite. *European Journal of Mineralogy* **7**, 1421–36.

**Fritz H, Abdelsalam M, Ali KA, Bingen B, Collins AS, Fowler AR, Ghebreab W, Hauzenberger CA, Johnson PR, Kusky TM, Macey PS, Muhongo P, Stern RJ and Viola G** (2013) Orogen styles in the East African Orogen: a review of the Neoproterozoic to Cambrian tectonic evolution. *Journal of African Earth Sciences* **86**, 65–106.

**Fritz H, Loizenbauer J and Wallbrecher E** (2014) Magmatic and solid state structures of the Abu Ziran pluton: deciphering transition from thrusting to extension in the Eastern Desert of Egypt. *Journal of African Earth Sciences* **99**, 122–35.

**Fritz H, Wallbrecher E, Khudeir AA, Abu El Ela F and Dallmeyer DR** (1996) Formation of Neoproterozoic metamorphic core complexes during oblique convergence (Eastern Desert, Egypt). *Journal of African Earth Sciences* **23**, 311–29.

**Gamble JA, Smith IEM, McCulloch MT, Graham IJ and Kokelaar BP** (1993) The geochemistry and petrogenesis of basalts from the Taupo Volcanic Zone and Kermadec Island Arc, SW Pacific. *Journal of Volcanology & Geothermal Research* **54**, 265–90.

**Green TH** (1972) Crystallization of calc-alkaline andesite under controlled high-pressure hydrous conditions. *Contributions to Mineralogy and Petrology* **34**, 150–66.

**Green TH and Ringwood AE** (1968) Genesis of the calc-alkaline igneous rock suite, *Contributions to Mineralogy and Petrology* **18**, 105–62.

**Greiling RO, Abdeen MM, Dardir AA, El Akhal H, El Ramly MF, Kamal El Din GM, Osman AF, Rashwan AA, Rice AHN and Sadek MF** (1994) A structural synthesis of the Proterozoic Arabian-Nubian Shield in Egypt. *Geologie Rundschau* **83**, 484–501.

**Greiling RO, Kröner A and El Ramly MF** (1984) Structural interference patterns and their origin in the Pan-African basement of the southeastern Desert of Egypt. *In Precambrian Tectonics Illustrated* (eds A. Kröner and R. O. Greiling), pp. 401–12. Stuttgart: Schweitzerbart'sche Verlagsbuchhandlung.

**Habib ME, Ahmed AA and El Nady OM** (1985) Tectonic evolution of the Meatiq infrastructure, central Eastern Desert, Egypt. *Tectonics* **4**, 613–27.

**Halla J, van Hunen J, Heilimo E and Hölttä P** (2009) Geochemical and numerical constraints on Neoarchean plate tectonics. *Precambrian Research* **179**, 155–62.

**Hawkesworth CJ, Gallagher K, Hergt JM and McDermott F** (1993) Mantle and slab contributions in arc magmas. *Annual Review of Earth & Planetary Sciences* **21**, 175–204.

**Hoffman PF** (1999) The break-up of Rodinia, birth of Gondwana, true polar wander and the snowball Earth. *Journal of African Earth Sciences* **28**, 17–33.

**Huang X-L, Niu Y, Xu Y-G, Yang Q-J and Zhong J-W** (2010) Geochemistry of TTG and TTG-like gneisses from Lushan-Taihua complex in the southern North China Craton: implications for late Archean crustal accretion. *Precambrian Research* **182**, 43–56.

**Hume WR** (1934) Geology of Egypt, the Fundamental Pre-Cambrian Rocks of Egypt and the Sudan, their Distribution, Age, and Character. Part 1. The Metamorphic Rocks, vol. 1. Cairo: Geological Survey of Egypt, 134 pp.

**Jarrar GH, Stern RJ, Saffarinai G and Al-Zubi H** (2003) Late- and post-orogenic Neoproterozoic intrusions of Jordan: implications for crustal growth in the northernmost segment of the East African Orogen. *Precambrian Research* **123**, 295–319.

**Jarrar GH, Theye T, Yaseen N, Whitehouse M, Pease V and Passchier C** (2013) Geochemistry and P-T-t evolution of the Abu-Barqa Metamorphic Suite, SW Jordan, and implications for the tectonics of the northern Arabian-Nubian Shield. *Precambrian Research* **239**, 56–78.

**Johnson PR, Andresen A, Collins AS, Fowler AR, Fritz H, Ghebrab W, Kusky T and Stern RJ** (2011) Late Cryogenian-Ediacaran history of the Arabian-Nubian Shield: a review of depositional, plutonic, structural, and tectonic event in the closing stages of the northern East African Orogen. *Journal of African Earth Sciences* **61**, 167–232.

**Johnson PR and Woldehaimanot B** (2003) Development of the Arabian-Nubian shield: perspectives on accretion and deformation in the northern East African Orogen and the assembly of Gondwana. In *Proterozoic East Gondwana: Supercontinent Assembly and Breakup* (eds M Yoshida, BE Windley and S Dasgupta), pp. 289–325. Geological Society of London, Special Publication no. 206.

**Küster D and Harms U** (1998) Post-collisional potassic granitoids from the southern and northwestern parts of the Late Neoproterozoic East African Orogen: a review. *Lithos* **45**, 177–95.

**Laurie A and Stevens G** (2012) Water-present eclogite melting to produce Earth's early felsic crust. *Chemical Geology* **314–317**, 83–95.

**Le Bas MJ and Streckeisen AL** (1991) The IUGS systematics of igneous rocks. *Journal of the Geological Society of London* **148**, 825–33.

**Loizenbauer J, Walbrecher E, Fritz H, Neumayr P, Khudeir AA and Kloetzli U** (2001) Structural geology, single zircon ages and fluid inclusion studies of

https://doi.org/10.1017/S0016756820000795 Published online by Cambridge University Press

the Meatiq metamorphic core complex: implications for Neoproterozoic tectonics in the Eastern Desert of Egypt. *Precambrian Research* **110**, 357–83.

**Lugmair GW and Marti K** (1978) Lunar initial $^{143}Nd/^{144}Nd$: differential evolution of the lunar crust and mantle. *Earth and Planetary Science Letters* **39**, 349–57.

**Marsh BD and Carmichael ISE** (1974) Benioff Zone Magmatism. *Journal of Geophysical Research* **79**, 1196–206.

**Martin H** (1987) Petrogenesis of Archean trondhjemites, tonalites, and granodiorites from Eastern Finland: major and trace element geochemistry. *Journal of Petrology* **28**, 921–53.

**Martin H** (1993) The mechanisms of petrogenesis of the Archean continental crust - comparison with modern processes. *Lithos* **30**, 373–88.

**Martin H** (1999) The adakitic magmas: modern analogues of Archaean granitoids. *Lithos* **46**, 411–29.

**Martin H, Smithies RH, Rapp R, Moyen J-F and Champion D** (2005) An overview of adakite, tonalite–trondhjemite–granodiorite (TTG) and sanukitoid: relationships and some implications for crustal evolution. *Lithos* **79**, 1–24.

**Mattinson JM** (2005) Zircon U–Pb chemical abrasion ("CA-TIMS") method: combined annealing and multi-step partial dissolution analysis for improved precision and accuracy of zircon ages. *Chemical Geology* **220**, 47–66.

**Maurice AE, Basta FF and Khiamy AA** (2012) Neoproterozoic nascent island arc volcanism from the Nubian shield of Egypt: magma genesis and generation of continental crust in intra-oceanic arcs. *Lithos* **132**, 1–20.

**McLean NM, Condon DJ, Schoene B and Bowring SA** (2015) Evaluating uncertainties in the calibration of isotopic reference materials and multi-element isotopic tracers (EARTHTIME Tracer Calibration Part II). *Geochimica et Cosmochimica Acta* **164**, 481–501.

**Meert JG and Lieberman BS** (2008) The Neoproterozoic assembly of Gondwana and its relationship to the Ediacaran - Cambrian radiation. *Gondwana Research* **14**, 5–21.

**Meert JG and Torsvik TH** (2003) The making and unmaking of a supercontinent: Rodinia revisited. *Tectonophysics* **375**, 261–88.

**Moyen J-F** (2009) High Sr/Y and La/Y ratios: the meaning of the "adakitic signature". *Lithos* **112**, 556–74.

**Moyen J-F** (2011) The composite Archaean grey gneisses: petrological significance, and evidence for a non-unique tectonic setting for Archaean crustal growth. *Lithos* **123**, 21–36.

**Moyen J-F and Martin H** (2012) Forty years of TTG research. *Lithos* **148**, 312–36.

**Moyen J-F and Stevens G** (2006) Experimental constraints on TTG petrogenesis: implications for Archean geodynamics. In *Archean Geodynamics and Environments* (eds K Benn, J-C Mareschal and KC Condie), pp. 149–78. American Geophysical Union, Washington, Monographs.

**Moyen J-F, Stevens G, Kisters AFM and Belcher RW** (2007) TTG plutons of the Barberton granitoid-greenstone terrain, South Africa. In *Earth's Oldest Rocks* (eds MJ Van Kranendonk, RH Smithies and V Bennet), pp. 606–68. Amsterdam: Elsevier, Developments in Precambrian Geology.

**Nagel TJ, Hoffmann JE and Münker C** (2012) Melting of Eoarchaean TTGs from thickened mafic arc crust. *Geology* **40**, 375–8.

**Nair R and Chacko T** (2008) Role of oceanic plateaus in the initiation of subduction and origin of continental crust. *Geology* **36**, 583–6.

**Nasseef MO, Bakor AR and Hashad AM** (1980) Petrography of possible ophiolitic rocks along the Qift-Quseir road, Eastern Desert, Egypt: evolution and mineralization of the Arabian Shield. *King Abdulaziz University, Institute of Applied Geology Bulletin* **3**, 157–68.

**Neubauer WH** (1962) Geologie der Goldlagerstagette von E1-Sid in Obseraegypten mit einem Beitriag zur Geologie der zentralen arabischen Wueste. *Geologische Jahrbuch* **80**, 117–25.

**Neumayr P, Hoinkes G, Puhl J, Mogessie A and Khudeir AA** (1998) The Meatiq dome (Eastern Desert, Egypt), a Precambrian metamorphic core complex: petrological and geological evidence. *Journal of Metamorphic Geology* **16**, 259–79.

**Neumayr P, Mogessie A, Hoinkes GP and Puhl J** (1996) Geological setting of the Meatiq metamorphic core complex in the Eastern Desert of Egypt based on amphibolite geochemistry. *Journal of African Earth Sciences* **23**, 331–45.

**O'Connor JT** (1965) A classification for quartz-rich igneous rocks based on feldspar ratios. *US Geological Survey Professional Paper* **525-B**, 79–84.

**Pearce JA, Harris NBW and Tindle AG** (1984) Trace element discrimination diagrams for the tectonic interpretation of granitic rocks. *Journal of Petrology* **25**, 956–83.

**Popov VS, Nikiforova NF and Bogatov VI** (2001) Multiple gabbro-granite intrusive series of the Syrostan pluton, southern Urals; geochemistry and petrology. *Geochemistry International* **39**, 732–47.

**Prouteau G, Scaillet B, Pichavant M and Maury RC** (2001) Evidence for mantle metasomatism by hydrous silicic melts derived from subducted oceanic crust. *Nature* **410**, 197–200.

**Rapp RP** (1994) Partial melting of metabasalts at 2–7 GPa: experimental results and implications for lower crustal and subduction zone processes. *Mineralogical Magazine* **58A**, 760–1.

**Rapp RP, Shimizu N and Norman MD** (2003) Growth of early continental crust by partial melting of eclogite. *Nature* **425**, 605–9.

**Rapp RP, Shimizu N, Norman MD and Applegate GS** (1999) Reaction between slab-derived melts and peridotite in the mantle wedge: experimental constraints at 3.8 GPa. *Chemical Geology* **160**, 335–56.

**Rapp RP and Watson EB** (1995) Dehydration melting of metabasalt at 8–32 kbar implications for continental growth and crust–mantle recycling. *Journal of Petrology* **36**, 891–931.

**Rapp RP, Watson EB and Miller CF** (1988) Experimental partial melting of amphibolite at 8-28 kbar: compositions of liquids and coexisting crystal residues (abstract). *Goldschmidt Conference Program and Abstracts*, 11–13 May 1988, Baltimore, Maryland: Geochemical Society. Abstract, p. 69.

**Rapp RP, Watson EB and Miller CF** (1991) Partial melting of amphibolite/eclogite and the origin of Archean trondhjemites and tonalities. *Precambrian Research* **51**, 1–25.

**Ries AC, Shackleton RM, Graham RH and Fitches WR** (1983) Pan-African structures, ophiolites and mélanges in the Eastern Desert of Egypt: a traverse at 26°N. *Journal of the Geological Society of London* **140**, 75–95.

**Robinson FA, Foden JD and Collins AS** (2015) Geochemical and isotopic constraints on island arc, synorogenic, post-orogenic and anorogenic granitoids in the Arabian Shield, Saudi Arabia. *Lithos* **220–223**, 97–115.

**Robinson FA, Foden JD, Collins AS and Payne JL** (2014) Arabian Shield magmatic cycles and their relationship with Gondwana assembly: insights from zircon U–Pb and Hf isotopes. *Earth and Planetary Science Letters* **408**, 207–25.

**Rollinson H** (1997) Eclogite xenoliths in west African kimberlites as residues from Archaean granitoid crust formation. *Nature* **389**, 173–76.

**Schmidt MW, Dardon A, Chazot G and Vannucci R** (2004) The dependence of Nb and Ta rutile-melt partitioning on melt composition and Nb/Ta fractionation during subduction processes. *Earth and Planetary Science Letters* **226**, 415–32.

**Schmidt MW and Poli S** (2004) Magmatic epidote. In *Epidotes* (eds A Liebscher and G Franz), pp. 399–430. Washington DC: Mineralogical Society of America and the Geochemical Society, Reviews in Mineralogy & Geochemistry, 56.

**Schmidt MW and Thompson AB** (1996) Epidote in calc-alkaline magmas: an experimental study of stability, phase relationships, and role of epidote in magmatic evolution. *American Mineralogist* **81**, 462–74.

**Schmitt AK, Emmermann R, Trumbull RB, BuÈhn B and Henjes-Kunst F** (2000) Petrogenesis and $^{40}Ar/^{39}Ar$ geochronology of the Brandberg complex, Namibia: evidence for a major mantle contribution in metaluminous and peralkaline granites. *Journal of Petrology* **41**, 1207–39.

**Schuermann HM** (1966) *The Pre-Cambrian along the Gulf of the Suez and the Northern Part of the Red Sea*. Leiden, Netherlands: EJ Brill, 76 pp.

**Senshu H, Maruyama S, Rino S and Santosh M** (2009) Role of tonalite-trodhjemite-granite (TTG) crust subduction on the mechanism of supercontinent breakup. *Gondwana Research* **15**, 433–42.

**Shackleton RM** (1996) The final collision zone between East and West Gondwana: where is it? *Journal of African Earth Sciences* **23**, 271–87.

**Shackleton RM, Ries AC, Graham RH and Fitches WR** (1980) Late Precambrian ophiolite melange in the Eastern Desert of Egypt. *Nature* **285**, 472–4.

**Smithies RH and Champion DC** (2000) The Archaean high-Mg diorite suite: links to tonalite–trondhjemite–granodiorite magmatism and implications for early Archaean crustal growth. *Journal of Petrology* **41**, 1653–71.

https://doi.org/10.1017/S0016756820000795 Published online by Cambridge University Press

**Souza ZS, Potrel H, Lafon JM, Althoff FJ, Pimentel MM, Dall'Agnol R and Oliveira CG** (2001) Nd, Pb and Sr isotopes of the Identidade Belt, an Archaean greenstone belt of the Rio Maria region (Carajas Province, Brazil): implications for the Archaean geodynamic evolution of the Amazonian Craton. *Precambrian Research* **109**, 293–315.

**Stacey JS and Kramers JD** (1975) Approximation of terrestrial lead isotope evolution by a 2-stage model. *Earth and Planetary Science Letters* **26**, 207–21.

**Steiger RH and Jäger E** (1977) Sub-commission on Geochronology: convention on the use of decay constants in geo- and cosmochronology. *Earth and Planetary Science Letters* **36**, 359–62.

**Stern RJ** (1994) Arc assembly and continental collision in the Neoproterozoic East African Orogen: implications for the consolidation of Gondwanaland. *Annual Reviews of Earth Planetary Sciences* **22**, 319–51.

**Sturchio NC, Sultan M and Batiza R** (1983) Geology and origin of the Meatiq Dome, Egypt: a Precambrian metamorphic core complex? *Geology* **11**, 72–6.

**Sun SS and McDonough WF** (1989) Chemical and isotopic systematics of oceanic basalts: implications for mantle composition and processes. In *Magnatism in Ocean Basins* (eds AS Saunders and MJ Norry), pp. 313–45. Geological Society of London, Special Publication no. 42.

**Teklay M, Berhe K, Reimold WU, Armstrong R, Asmerom Y and Watson J** (2002a) Geochemistry and geochronology of a Neoproterozoic low-K tholeiite-boninite association in Central Eritrea. *Gondwana Research* **5**, 597–61.

**Teklay M, Kröner A and Mezger K** (2002b) Enrichment from plume interaction in the generation of Neoproterozoic arc rocks in northern Eritrea: implications for crustal accretion in the southern Arabian–Nubian Shield. *Chemical Geology* **184**, 167–84.

**Tohver E, D'Agrella MS and Trindade RJF** (2006) Paleomagnetic record of Africa and South America for the 1200-500 Ma interval, and evaluation of Radinia and Gondwana assemblies. *Precambrian Research* **147**, 193–222.

**Vail JR** (1990) *Geochronology of the Sudan*. London: British Geological Survey, Overseas Geology and Mineral Resources issue 66, 59p.

**van Hunen J and Moyen J-F** (2012) Archaean subduction: fact or fiction? *Annual Review of Earth and Planetary Sciences* **40**, 195–219.

**Wilson T, Grunow AM and Hanson RE** (1997) Gondwana Assembly: the view from southern Africa and East Gondwana. *Journal of Geodynamics* **23**, 263–86.

**Winther KT** (1996) An experimentally based model for the origin of tonalitic and trondhjemitic melts. *Chemical Geology* **127**, 43–59.

**Wolf MB and Wyllie PJ** (1989) The formation of tonalitic liquids during the vapor-absent partial melting of amphibolite at 10 kb (abstract). *Eos, Transactions of American Geophysical Union* **70**, 506.

**Wolf MB and Wyllie PJ** (1994) Dehydration-melting of amphibolite at 10 kbar: the effects of temperature and time. *Contributions to Mineralogy and Petrology* **115**, 369–83.

**Woodhead JD** (1989) Geochemistry of the Mariana arc (Western Pacific): source composition and processes. *Chemical Geology* **76**, 1–24.

**Wylie PJ, Wolf MB and van der Laan SR** (1997) Conditions for formation of tonalites and trondhjemites: magmatic sources and products. In *Greenstone Belts* (eds M De Wit and LD Ashwal), pp. 256–66. Oxford: Oxford University Press.

**Xiong XL, Adam J and Green TH** (2005) Rutile stability and rutile/melt HFSE partitioning during partial melting of hydrous basalt: implications for TTG genesis. *Chemical Geology* **218**, 339–59.

**Zen E-An and Hammarstorm JM** (1984) Magmatic epidote and its petrologic significance. *Geology* **12**, 515–18.

https://doi.org/10.1017/S0016756820000795 Published online by Cambridge University Press